Report on a problem studied at the UK Mathematics-in-Medicine Study Group Oxford 2005
< http://www.maths-in-medicine.org/uk/2005/biofilms/ >

Modelling the development and formation of biofilms

John Ward (Loughborough University), Jonathan Wattis, Sara Jabbari, Jennifer Siggers (University of Nottingham), Ryo Kabayashi (Hiroshima University), Judith Armitage (University of Oxford) and Scott Godfrey, Helen Packer (Oxford Brookes University).

Abstract

Biofilms are bacterial colonies growing on solid-fluid interfaces. Planktonic (swimming) bacteria attach to a surface and develop into a microcolony through cell division. In time, through the bacterial production of exo-polysaccharides, they mature to form highly complex and highly heterogeneous structures which are notoriously resistant to anti-microbial agents. Through sloughing, the bacteria are able to spread and recolonise elsewhere. The biofilms of the bacterium *Rhodobacter sphaeroides* have additional characteristics: 1) they form bacterial chains in the early stages and 2) individual planktonic cells (regulated by quorum sensing) disperse from the biofilm surface.

In this report, four mathematical models are investigated. Firstly the role of growth and cleavage in chain formation is investigated and steady-state analysis reveals a range of distributions that could help identify key mechanisms given appropriate data. The role of nutrient diffusion in the biofilm morphology is investigated by two models, suggesting that the observed structures can be explained by nutrient limitations alone. The role of quorum sensing (QS) and planktonic cell dispersal on biofilm growth is investigated in the fourth model, where a sufficient condition for QS activity is derived, but suggests that mechanisms other than planktonic cell escape are needed to explain the observed limits in biofilm growth.

1 Introduction

1.1 Bacterial biofilm formation

There has been a dramatic change in our conceptual understanding of bacterial modes of existence in natural environments over the last 20-25 years brought about by the realisation that the predominant microbial lifestyle is not one of free swimming (planktonic) individuals, but as members of complex surface attached communities called biofilms [7]. Since this realisation, intense efforts spanning multiple disciplines have been initiated with an aim to understanding the nature of this ubiquitous microbial lifestyle in which bacteria enclosed within biofilms are physiologically and metabolically distinct from their planktonic counterparts.

1.1.1 Biofilm structure and development

Environmental microbiologists have long recognised that complex bacterial communities exist; recently, advances in microscopy and molecular technologies made it possible to closely examine such communities in situ. Biofilm formation has been studied with the use of flowing and stationary systems enabling the investigation of the structures of biofilms and their physical properties [8, 15, 16]. Biofilm development initiates when bacteria undergo a transition from a planktonic state to that of firmly attached cells on biotic or abiotic surfaces. Initial attachment is thought to be regulated in part by the nutritional status of the environment [29]. After

the initial attachment to the substratum, cells are thought to undergo a program of physiological changes that result in a highly structured microbial community. Through growth and active movement across the substratum, spatially distinct clusters of cells, referred to as microcolonies, are formed [19]. Although biofilms are highly structured, they are not permanent. Sloughing of cells from the mature biofilm (*i.e* shedding of biofilm material from the surface can occur though death, degradation or by cell-mediated mechanisms [19, 26]. This sloughing of cells acts as a means of colonising new surfaces so as to avoid population-density-mediated starvation of attached bacterial communities [2]. Detached cells re-enter a planktonic phase, and the developmental cycle effectively begins again. This generalised overview of biofilm formation and structure is intended to provide a framework for further discussions (Figure 1).

1.1.2 Quorum sensing within biofilms

In recent years, advances in technology has greatly increased the resolution of biofilm investigation and studies are providing valuable and intriguing information on the complexity of interaction between cells in the biofilm - none more so than the process known as quorum-sensing. Bacteria have been shown to be able to coordinate their activities through the production of acylated homoserine lactones (AHLs) [12]. These small membrane-permeable signal molecules accumulate in cultures in a cell-density-dependent relationship. Upon reaching a threshold local concentration (the quorum), AHLs can interact with specific receptors that signal the bacteria to activate differential sets of genes. In effect, quorum sensing allows coordinated gene expression that is regulated by cell density. These systems are widespread and have been linked to the regulation of diverse functions. For example, quorum-sensing systems are known to be involved in the regulation of virulence genes in *Pseudomonas aeruginosa*, conjugal transfer in *Agrobacterium tumefaciens*, swarming motility in *Serratia liquefaciens* and antibiotic production in *Erwinia caratovora* [13, 22].

1.1.3 *Rhodobacter sphaeroides* and biofilm development

The alpha subgroup bacterium *R. sphaeroides* WS8 is a widely dispersed, motile, purple non-sulphur bacterium with a versatile metabolism, using anaerobic and aerobic respiration or photoheterotrophims as energy sources for growth. It can also grow as a photoautolithotroph with carbon dioxide as the sole carbon source and in addition can fix nitrogen. Its metabolic versatility enables it to colonise many different niches in the environment. This purple non-sulphur bacterium is one of the most understood non-enteric bacteria, as it has been widely studied due to its remarkable genomic and physiologic complexity.

R. sphaeroides has been shown to be an important primary coloniser of surfaces in coastal waters [9]. Such primary colonisers establish the initial particle surface-colonising assemblage by changing the physio-chemical properties of the surface, particularly by exopolysaccharide production, making the surface more, or sometimes less, suitable for recruitment of later colonists.

R. sphaeroides is motile, propelling itself by a single flagellum that is controlled by a complex chemosensory system containing multiple homologues of the classical *E. coli* chemotaxis pathway. This more complex pathway appears to be finely tuned to respond to very small changes in a diverse range of signals, including metabolic changes, to drive motility towards the optimum conditions for metabolism, growth and survival [18, 24].

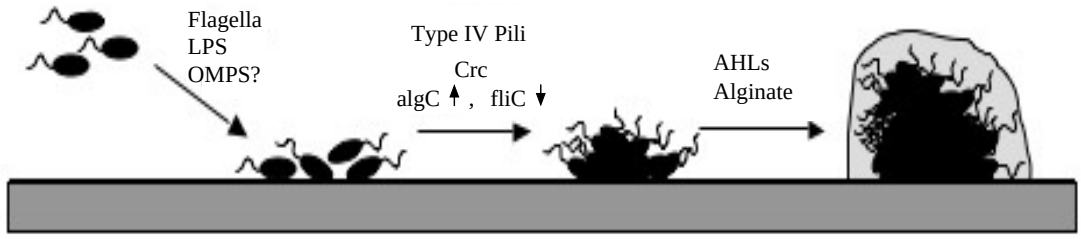

Figure 1: Biofilm development in Gram-negative organisms [10]. This figure outlines the current model for early stages in biofilm formation in *P. aeruginosa*. From left to right: Flagella are required to bring the bacterium into proximity with the surface, and LPS (lipopolysaccharide, a component of the bacterium's outer membrane) mediates early interactions, with an additional possible role for outer membrane proteins (OMPs). Once on the surface in a monolayer, type IV pilus-mediated twitching motility is required for the cells to aggregate into microcolonies. The production of pili is regulated at least in part by nutritional signals via Crc. Documented changes in gene expression at this early stage include upregulation of the alginate biosynthesis genes and downregulation of the flagella synthesis. The production of cell-to-cell signalling molecules (AHLs) is required for formation of the mature biofilm and alginate may also play a structural role in this process [10].

The chemosensory system and motility are widely accepted as having a role in biofilm formation and dispersal. *In vitro* flow cell studies and microcosms have shown that *R. sphaeroides* has the ability to form morphologically distinct biofilms when growth conditions are altered (Godfrey & Packer *et al.* unpublished data).

R. sphaeroides biofilm development follows the typical scenario depicted with *P. aeruginosa* (Figure 1) with a noticeable exception in that chains of cells are observed on the surface of the film following early biofilm attachment. Microscopy studies using confocal scanning laser microscopy have observed that biofilm structural development by *R. sphaeroides* follows the model proposed in Figure 2. Within 24-48 hours, many chains and single motile cells are observed to aggregate together to form microcolonies. The microcolonies develop into a mature biofilm as a result of up-regulated exopolysaccharide (EPS) production that encases and binds the cells together. Mature biofilm establishment leads to the dissociation of the chains within the EPS matrix resulting in a predomination of individual cells (with few chains) within the mature biofilm (Figure 2). R. sphaeroides produces a long chain AHL molecule (C14) and experimental evidence shows that strains deficient in the production of this AHL exhibit cellular clumping in liquid culture [21]. Therefore it seems possible that in R. sphaeroides, AHL is a regulatory mechanism enabling dissociation of chains into single cells (as observed in the mature biofilm) and also regulation of motile planktonic cell dispersal from a mature biofilm when the quorum is reached (Figure 2).

1.2 Outline of the sections to follow

In the next four sections, a number of the aspects of biofilm formation and development discussed above will be investigated using mathematical modelling. In Section 2 (by J. Wattis

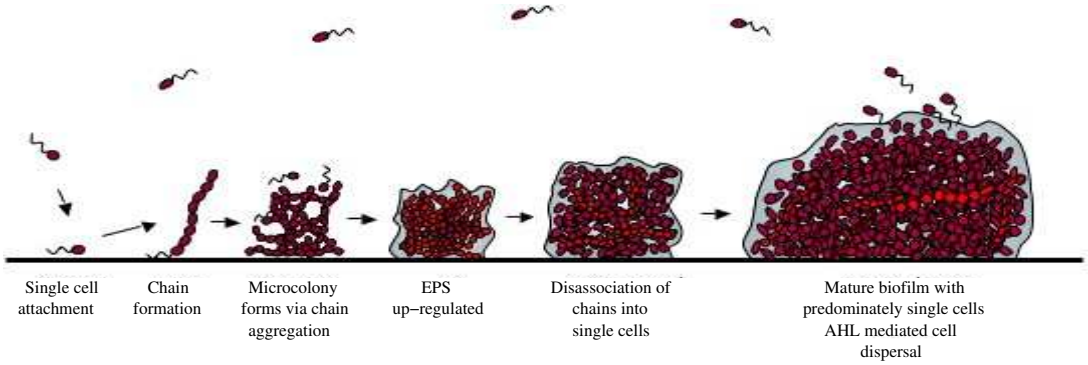

Figure 2: Proposed model of *Rhodobacter sphaeroides* biofilm formation. From left to right: planktonic bacteria attach themselves on to a solid surface and over the course of a few hours form cell chains. Eventually, these chains aggregate to form microcolonies and, in time, through the production of EPS and the chain breakup, the biofilm develops in a similar fashion to that described in Figure 1. In mature biofilms, perhaps mediated by quorum sensing, individual cells at the surface become planktonic and escape into the fluid media to colonise elsewhere.

and S. Jabbari), the chain formation during the early stages of *R. sphaeroides*' biofilm development is investigated. Then in Sections 3 (J. Siggers) and 4 (R. Kabayashi), the role of nutrient transport on biofilm morphology is investigated, starting with the initial formation of "pillars" due to nutrient diffusion-driven instabilities and then how the growth of these pillars are effected by the flow of the fluid media. The role of planktonic cell dispersal and quorum sensing, relevant for *R. sphaeroides* biofilms, are investigated in Section 5 (J. Ward). Finally, an overview of the work is discussed in the Section 6.

2 Modelling chain formation

The observation that individual *Rhodobacter sphaeroides* cells form chains in the initial stages of biofilm formation is relatively recent. Hence little is known about the structure of these chains or how they form. Under normal circumstances, each bacterial cell undergoes binary fission after a certain amount of time in order to reproduce. They divide to produce two new daughter cells which split away from each other to form a pair of distinct cells. What is known about the formation of these *Rhodobacter* chains is that the division process begins, but as a result of some unknown mechanism, is never quite completed. Two new daughter cells form but do not succeed in breaking away from each other, resulting in a chain of two cells. As this division process continues in these cells, the chain grows longer and longer. Thus, each chain contains cells which all originate from the same parent cell.

It is unclear, however, which cells continue to divide. Is it every cell in the chain, or only a certain number of cells, for example only the end cells? Also, since very long chains have not yet been observed, can the chains break? Can they shed their end cells?

We have modelled an approximation of the steady state distribution of chain lengths. In this we include cell division, and allow for the possibility that chains can break and shed their end cells. We chose to investigate four possibilities:

Case I Only the end cells of the chain divide and all chains are equally likely to break

(irrespective of length)

Case II All cells in the chain divide and all chains are equally likely to break

Case III Only the end cells of the chain divide and longer chains are more likely to break

Case IV All cells in the chain divide and longer chains are more likely to break

In each case we let c_r be the number density of chains of length r and construct differential-difference equations using the mechanisms which we believe to be involved in chain formation, that is, cell division, shedding of the end cell of a chain as it becomes planktonic, and sloughing of a large fragment of a chain. For this we need the following parameters:

a: rate of cell division,

b: rate of shedding, that is the loss of a single cell from the end of a chain,

k: rate of sloughing, that is, the rate at which chains break or fragment at some point in the interior of the chain (also known as chain scission).

Each of the above rate constants may depend on chain length (r). The basic model of chain growth and shedding has a similar form to the Becker-Doring system of equations [5], that is chains grow $C_r \to C_{r+1}$ at a rate a_r and decay $C_r \to C_{r-1}$ at a rate b_r thus we obtain

$$\frac{\mathrm{d}c_r}{\mathrm{d}t} = a_{r-1}c_{r-1} - a_r c_r - b_r c_r + b_{r+1}c_{r+1}, \qquad (r \geq 2) \tag{1}$$

with a modified equation governing the behaviour of c_1. We assume that the new cells generated from cell division are created *ex nihilo* and do not deplete the stock of chains of unit length, and that the planktonic cells released from the end of the chains also are swept out of the system. To obtain physically realistic solutions the rate of chain growth a_r must not grow faster than linearly in r; for the case $a_r = a$ independent of r, and the case $a_r = ar$, exact solutions are available (see [6, 14, 28]).

To the system (1) we add in the fragmentation term from a binary fragmentation model, which arises in reversible Smoluchowski coagulation [23, 3][1], namely $C_r \to C_s + C_{r-s}$ at a rate $k_{s,r-s}$. We assume that both fragments are retained in the experimental apparatus as long chains will easily be caught up in other colonies, or may even attach to the substrate and start a new colony. Thus we obtain the general model

$$\frac{\mathrm{d}c_r}{\mathrm{d}t} = a_{r-1}c_{r-1} - a_r c_r - b_r c_r + b_{r+1}c_{r+1} - \frac{1}{2}\left(\sum_{s=1}^{r-1} k_{s,r-s}\right) c_r + \sum_{s=1}^{\infty} k_{r,s}c_{r+s}, \qquad (r \geq 2). \tag{2}$$

The equation for chains of length one is

$$\frac{\mathrm{d}c_1}{\mathrm{d}t} = J - a_1 c_1 + b_2 c_2 + \sum_{s=1}^{\infty} k_{s,1}c_{s+1}, \tag{3}$$

where J is the net rate at which bacteria adhere to the surface from the environment. In a clean flow this might be zero; however, if there are other bacterial communities upstream

[1]The reversible Smoluchowski coagulation equations are

$$\frac{\mathrm{d}c_r}{\mathrm{d}t} = \frac{1}{2}\sum_{s=1}^{r-1}\left(k^f_{s,r-s}c_s c_{r-s} - k^r_{s,r-s}c_r\right) - \sum_{s=1}^{\infty}\left(k^f_{r,s}c_r c_s - k^r_{r,s}c_{r+s}\right),$$

in (2) we set $k^f_{r,s} = 0$, retaining just the $k^r_{r,s}$ terms.

which are shedding cells at a rate q, then J might have the form $\lambda q - \mu c_1$, where λ is the adherence rate and μ is a removal rate. In the analysis below we seek steady-state solutions, and so we implicitly assume that c_1 also maintains a steady value.

Such mixed Becker-Doring-Smoluchowski systems have occasionally been analysed before, for example in the model of RNA chain polymerisation [27], where the focus was on solutions which led to concentrations which grew in time. Here, we shall simply seek steady solutions, that is, distributions of chain-length which are time-independent. We typically expect the rate coefficient $k_{r,s}$ to be much smaller than b_r and a_r.

Below we shall assume forms for the rate constants a_r and $k_{r,s}$, which are either independent of chain length or proportional to chain length. The shedding rate b_r will always be assumed to be independent of chain length, that is $b_r = b$. We assume the existence of a significant number of long chains, so that the chain length parameter (r) may be taken as a continuous variable. We then take the continuum limit of the governing equations to obtain a second order differential equation for each case which can then be solved to approximate the steady state distributions of chain lengths in each case.

2.1 Case I

In this case we assume that only the cells at each end of a chain divide, thus the rate of chain growth is the same for all chains, $a_r = a$. We assume that the end cells may also become planktonic and swim off into the environment, causing the chains to reduce in length; we denote the rate at which this occurs by b –independent of r. In addition, we assume that a chain may fracture at some point along its length and a large fragment be lost, this occurs at some rate k, which, in this case, we assume to be independent of chain length. This corresponds to assuming that $k = \frac{1}{2}\sum_{s=1}^{r-1} k_{s,r-s}$ in (2); the simplest fragmentation kernel $k_{r,s}$ which satisfies this is $k_{r,s} = 2k/(r+s-1)$ so that $k_{s,r-s} = 2k/(r-1)$. To obtain a viable population of chains of a significant length, we assume that the growth rate a will exceed b. The appropriate differential-difference equation for the concentration of chains of length r at time t is thus

$$\frac{\mathrm{d}c_r}{\mathrm{d}t} = ac_{r-1} - ac_r - bc_r + bc_{r+1} + k\sum_{s=1}^{\infty} \frac{2c_{r+s}}{r+s-1} - kc_r. \tag{4}$$

In order to investigate the shape of the chain length distribution $c_r(t)$ at large lengths (r), we let $x = hr$, where $h \ll 1$, and introduce $\tilde{c}(x,t) = c_r(t)$. Using a Taylor series expansion in x, we obtain the partial differential equation

$$\frac{\partial \tilde{c}(x,t)}{\partial t} = (b-a)h\frac{\partial \tilde{c}}{\partial x} + 2k\int_{y=x}^{\infty} \frac{\tilde{c}(y,t)}{y}\,\mathrm{d}y - k\tilde{c}. \tag{5}$$

To obtain a solution in which growth shedding and sloughing are all relevant, we note that k is expected to be small so we write $k = h\kappa$. Taking $h \to 0$, the equation for the steady-state $c^{\mathrm{sss}}(x) = \tilde{c}(x,t)$ is then

$$0 = (b-a)c^{\mathrm{sss}\prime}(x) + 2\kappa\int_{x}^{\infty} \frac{c^{\mathrm{sss}}(y)}{y}\,\mathrm{d}y - \kappa c^{\mathrm{sss}}(x). \tag{6}$$

This is equivalent to

$$0 = (b-a)xc^{\mathrm{sss}\prime\prime} - \kappa x c^{\mathrm{sss}\prime} - 2\kappa c^{\mathrm{sss}}, \tag{7}$$

which has the general solution

$$\begin{aligned} c^{\text{sss}}(x) &= C_1 \mathrm{e}^{-\kappa x/(a-b)} x(2a-2b-\kappa x) \\ &\quad + C_2 \left[\kappa \mathrm{e}^{-\kappa x/(a-b)} x(2a-2b-\kappa x) E_1\left(\frac{-\kappa x}{a-b}\right) - (a-b)(a-b-\kappa x) \right], \end{aligned} \tag{8}$$

where $E_1(\cdot)$ is an Exponential integral function [1]. Such distributions are illustrated in Figures 3a and 4a. The solution $C_2 = 0$ has a particularly simple form; if $\kappa > 0$, then we have positive concentrations of chains of length zero up to $x_{\max} = 2(a-b)/\kappa$.

2.2 Case II

This case is identical to Case I in respect to chain fracture (sloughing, with rate $k_{r,s}$) and the shedding of end cells (as cells transform to the planktonic state); however, we consider the alternative growth hypothesis where all cells in a chain are permitted to undergo cell-division. The growth rate of a chain is thus proportional to the number of cells in it, and thus to its length, that is, $a_r = ar$ (in place of $a_r = a$). The governing equations are altered from (4) to

$$\frac{\mathrm{d}c_r}{\mathrm{d}t} = a(r-1)c_{r-1} - arc_r - bc_r + bc_{r+1} + k\sum_{s=1}^{\infty} \frac{2c_{r+s}}{r+s-1} - kc_r, \tag{9}$$

Again, we substitute $\tilde{c}(x,t) = c_r(t)$ with $x = hr$ and $h \ll 1$, then use a Taylor expansion to reduce equation (9) to the partial differential equation

$$\frac{\partial \tilde{c}}{\partial t} = -ax\frac{\partial \tilde{c}}{\partial x} - a\tilde{c} + bh\frac{\partial \tilde{c}}{\partial x} - k\tilde{c} + 2k\int_{y=x}^{\infty} \frac{\tilde{c}(y)}{y}\,\mathrm{d}y. \tag{10}$$

As in Case I, we expect k to be much smaller than b thus we write $k = h\kappa$; the typical growth rate is $a_r = ar = ax/h$, thus we expect the constant a also to be small, and so we make the substitution $a = h\alpha$.

We seek a steady-state solution to this equation. and therefore obtain the following approximation

$$0 = x[(b-\alpha x)c^{\text{sss}}(x)]'' - \kappa x c^{\text{sss}\prime}(x) - 2\kappa c^{\text{sss}}(x). \tag{11}$$

The solution to this differential equation is a linear combination of hypergeometric functions [1]

$$c^{\text{sss}}(x) = \frac{C_1 x}{|b-\alpha x|^{1+\kappa/\alpha}}\ {}_2F_1\left(\gamma_+, \gamma_-; -\frac{\kappa}{\alpha}; 1-\frac{\alpha x}{b}\right) + C_2 x\ {}_2F_1\left(2-\gamma_+, 2-\gamma_-; 2+\frac{\kappa}{\alpha}; 1-\frac{\alpha x}{b}\right). \tag{12}$$

where $\gamma_\pm = \frac{1}{2}(1-\kappa/\alpha \pm \sqrt{1-6\kappa/\alpha+\kappa^2/\alpha^2})$. In the case $b = 0$ the solution (12) simplifies to $c^{\text{sss}}(x) = C_1 x^{\gamma_+ - 1} + C_2 x^{\gamma_- - 1}$.

2.3 Case III

We now revert to the assumption that chains grow only by the end cells dividing, thus all chains have the same growth rate, $a_r = a$, irresepective of chain length. However, we modify Case I by assigning longer chains a higher rate of scission, that is, the rate at which a chain fragments depends on the number of cell-cell junctions, hence the term $\sum_{s=1}^{r-1} k_{s,r-s}$ in (2) depends on $r-1$. The simplest form arises from $k_{r,s} = k$ and leads to the governing equations

$$\dot{c}_r = ac_{r-1} - ac_r - bc_r + bc_{r+1} + 2k\sum_{s=1}^{\infty} c_{r+s} - k(r-1)c_r, \tag{13}$$

Once again approximating these by a continuum limit partial differential equation for $\tilde{c}(x,t) = \tilde{c}(hr,t) = c_r(t)$ with $h \ll 1$ gives

$$\frac{\partial \tilde{c}}{\partial t} = h(b-a)\frac{\partial \tilde{c}}{\partial x} + \frac{2k}{h}\int_{y=x}^{\infty} \tilde{c}(y,t)\,\mathrm{d}y - \frac{kx\tilde{c}}{h}. \tag{14}$$

As with Case I, we expect k to be much smaller than a and b; however, in this case, since $r = x/h$ and $x = \mathcal{O}(1)$, the typical value of the fragmentation term is k/h thus we write $k = h^2\kappa$. We seek a steady-state solution for $c^{\mathrm{sss}}(x) = \tilde{c}(x,t)$, which does not depend upon h, thus we let $h \to 0$ to eliminate all the higher-order correction terms. Differentiating (14) with respect to x we obtain the equation

$$0 = (b-a)\frac{\mathrm{d}^2 c^{\mathrm{sss}}}{\mathrm{d}x^2} - \kappa x\frac{\mathrm{d}c^{\mathrm{sss}}}{\mathrm{d}x} - 3\kappa c^{\mathrm{sss}}. \tag{15}$$

This has the general solution

$$\begin{aligned} c^{\mathrm{sss}}(x) \;=\; & C_1 \mathrm{e}^{-\kappa x^2/2(a-b)}\left(1 - \frac{\kappa x^2}{a-b}\right) + \\ & + C_2\left[\sqrt{2\pi}\,\mathrm{e}^{-\kappa x^2/2(a-b)}\left(1-\frac{\kappa x^2}{a-b}\right)\mathrm{erfi}\left(\frac{x}{2}\sqrt{\frac{2\kappa}{a-b}}\right) + 2x\sqrt{\frac{\kappa}{a-b}}\,\right], \end{aligned} \tag{16}$$

where $\mathrm{erfi}(z) = -i\,\mathrm{erf}(i\,z) = (2/\sqrt{\pi})\int_{t=0}^{z}\mathrm{e}^{t^2}\,\mathrm{d}t$. As in Case I, since chains grow only when the end cells divide (which occurs at rate a), but are reduced in length both by shedding (which occurs at rate b) and by sloughing; we expect $a > b$ in order to maintain a population of longer chains. If $C_2 = 0$ then the solution has a particularly simple form, which gives a distribution of chain lengths which decays monotonically with length, and has a maximum length of $x_{\max} = \sqrt{(a-b)/\kappa}$.

2.4 Case IV

This scenario is a combination of the two previous cases, in that both chain growth and chain fragmentation are proportional to chain length. The appropriate differential difference equations are

$$\dot{c}_r = a(r-1)c_{r-1} - arc_r - bc_r + bc_{r+1} + 2k\sum_{s=1}^{\infty} c_{r+s} - k(r-1)c_r, \tag{17}$$

The approximation to the steady state distribution $c^{\mathrm{sss}}(x)$ is

$$0 = [(h^2 b - ahx)c^{\mathrm{sss}}(x)]'' - kxc^{\mathrm{sss}\prime}(x) - 3kc^{\mathrm{sss}}(x), \tag{18}$$

thus we choose $a = h\alpha$ and $k = h^2\kappa$. The general solution is then

$$c^{\mathrm{sss}}(x) = C_1 \mathrm{M}\left(3, 2 + \frac{\kappa b}{\alpha^2}, \frac{\kappa}{\alpha}\left(\frac{b}{\alpha} - x\right)\right) + C_2 \mathrm{U}\left(3, 2 + \frac{\kappa b}{\alpha^2}, \frac{\kappa}{\alpha}\left(\frac{b}{\alpha} - x\right)\right). \tag{19}$$

Here the functions $M(\cdot,\cdot,z)$ and $U(\cdot,\cdot,z)$ are Kummer's hypergeometric functions, see Abramowitz & Stegun [1] for details. As with all the cases, our choice of parameters and boundary conditions will greatly influence the complexity of the resulting distribution. For example if the second argument is twice the first, then there are simplifications whereby M and U can be written in terms of Bessel functions (see Section 13.6 of [1]). More simply, if $\alpha^2 = b\kappa$ then $M(3,3,z) = \mathrm{e}^z$; the solution with $C_2 = 0$ has the form $\tilde{c}(x) = C_1\mathrm{e}^{1-\kappa x/\alpha}$. In this case there is no maximum chain length.

2.5 Comparing the four cases

We now have four distinct second order differential equations representing the steady state distributions of chain lengths in each case. Since we do not have the appropriate data to provide numerical values for a, b or k, we here illustrate qualitatively the forms of solutions to these equations to show that the four cases give rise to distributions which are clearly different shapes. We want $c^{\text{SSS}}(x_{\max}) = 0$ where $x_{\max}$ is some upper limit on chain lengths; in a couple of cases we have seen that $x_{\max}$ is finite, and in other cases infinite. For the cases where $x_{\max}$ is finite, we take it to be 10 and choose the amplitude scaling such that the largest concentration

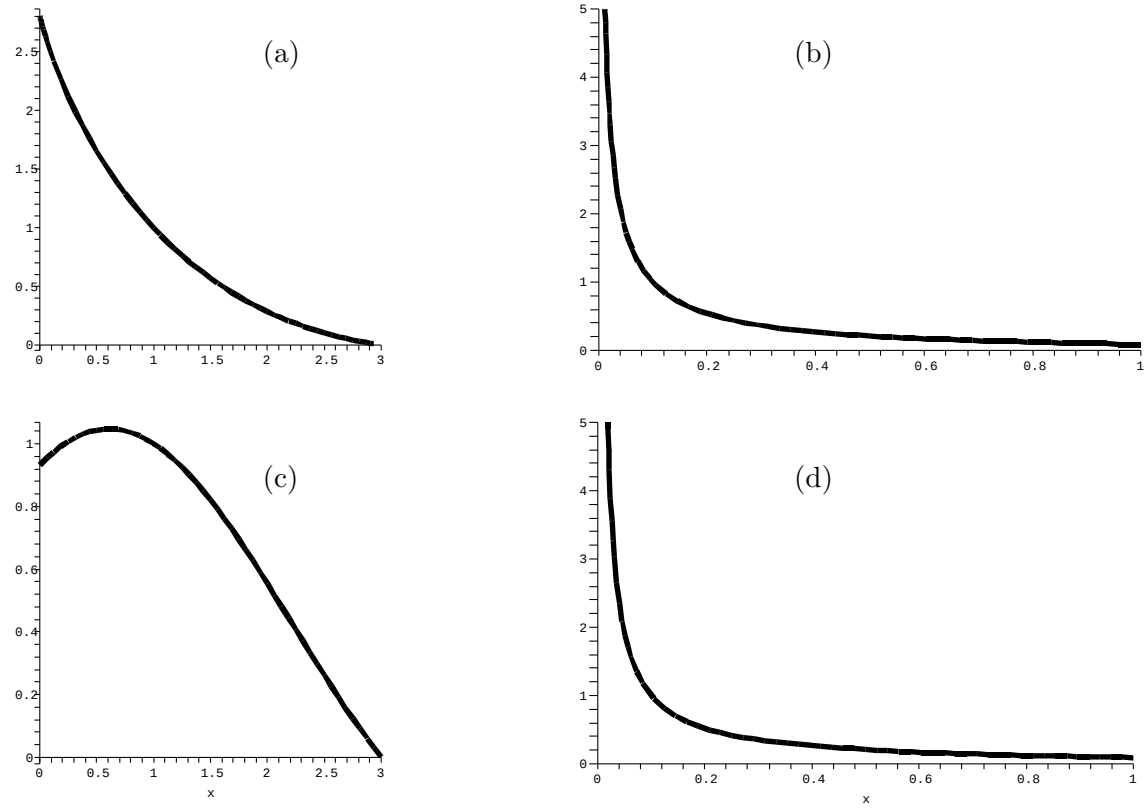

Figure 3: Graphs of the steady-state size distribution $c^{\text{SSS}}(x)$ againts x. (a) Case I, solution to Equation (8) with $a = 10$, $b = 0$, $\kappa = 1$, $c^{\text{SSS}}(1) = 1$, $c^{\text{SSS}}(3) = 0$. (b) Case II, solution to Equation (12) with $\alpha = 5$, $b = 0$, $\kappa = 1$, $c^{\text{SSS}}(0.1) = 1$, $c^{\text{SSS}}(3) = 0$. (c) Case III, solution to Equation (16) with $a = 5$, $b = 0$, $\kappa = 1$, $c^{\text{SSS}}(1) = 1$, $c^{\text{SSS}}(3) = 0$. (d) Case IV, solution to Equation (19) with $\alpha = 5$, $b = 0$, $\kappa = 1$, $c^{\text{SSS}}(0.1) = 1$, $c^{\text{SSS}}(3) = 0$.

In Figure 3 we illustrate the simple case where there is chain growth and sloughing, but no shedding. It must be remembered, however, that each of these parameters are scaled differently with h in each case so that they are not in fact equivalent parameters; they are chosen simply to demonstrate the different resulting distributions. We see that Cases II and IV are very similar, but that Cases I, II and III are all produce distinctly shaped distributions.

We see in Figure 4 that a variety of differently-shaped distributions are produced by the models, suggesting that if the appropriate experimental data were available, it would be possible to eliminate some models, and hence those mechanisms of growth and sloughing involved could be identified. Comparing Figures 3 and 4 shows the effect of shedding. As expected, shedding reduces the frequency of long chains and increases the frequency of shorter

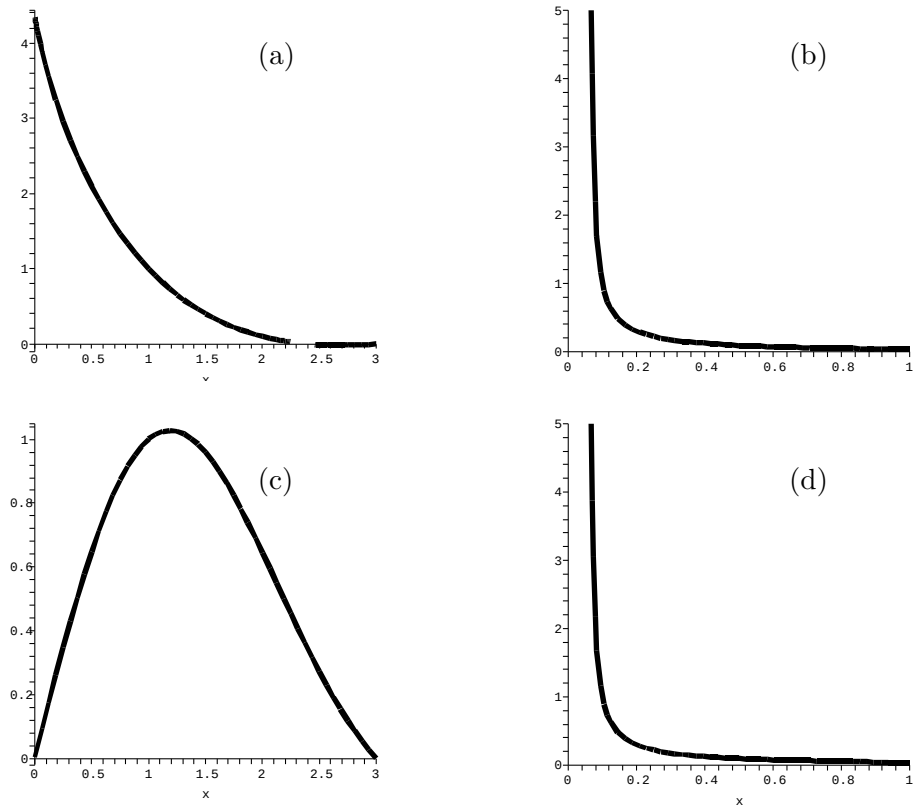

Figure 4: Replotting the steady-state distributions $c^{\text{SSS}}(x)$ against x as in Figure 3 but now with b non-zero to see the effect of shedding. (a) Case I, solution to Equation (8) with $a = 10$, $b = 3$, $\kappa = 1$, $c^{\text{SSS}}(1) = 1$, $c^{\text{SSS}}(3) = 0$. (b) Case II, solution to Equation (12) with $\alpha = 5$, $b = 0.3$, $\kappa = 1$, $c^{\text{SSS}}(0.1) = 1$, $c^{\text{SSS}}(3) = 0$. (c) Case III, solution to Equation (16) with $a = 5$, $b = 3$, $\kappa = 1$, $c^{\text{SSS}}(1) = 1$, $c^{\text{SSS}}(3) = 0$. (d) Case IV, solution to Equation (19) with $\alpha = 5$, $b = 0.3$, $\kappa = 1$, $c^{\text{SSS}}(0.1) = 1$, $c^{\text{SSS}}(3) = 0$.

chains - this is most apparent in cases I, II and IV. The change in shape of Case III is most surprising. It is partly due to the choice of normalisation, we have chosen to use $c^{\text{SSS}}(1) = 1$ and $c^{\text{SSS}}(3) = 0$ for both $b = 0$ and $b > 0$ whereas, in the presence of shedding ($b > 0$), we might expect the distribution to reach zero concentration at a lower value of chain length, x.

In three of the four cases we have studied, there is a particularly simple solution. In Cases I, II and IV we have the steady-state solutions

$$c_r^{\text{SSSI}} = Cr(2a - 2b - kr)\mathrm{e}^{-kr/(a-b)}, \tag{20}$$

$$c_r^{\text{SSSIII}} = C\left(1 - \frac{kr^2}{a-b}\right)\mathrm{e}^{-kr^2/2(a-b)}, \tag{21}$$

$$c_r^{\text{SSSIV}} = C\mathrm{e}^{1-kr/a} \tag{22}$$

with the solution for Case IV only being valid if $a^2 = bk$. These special solutions are illustrated in Figure 5.

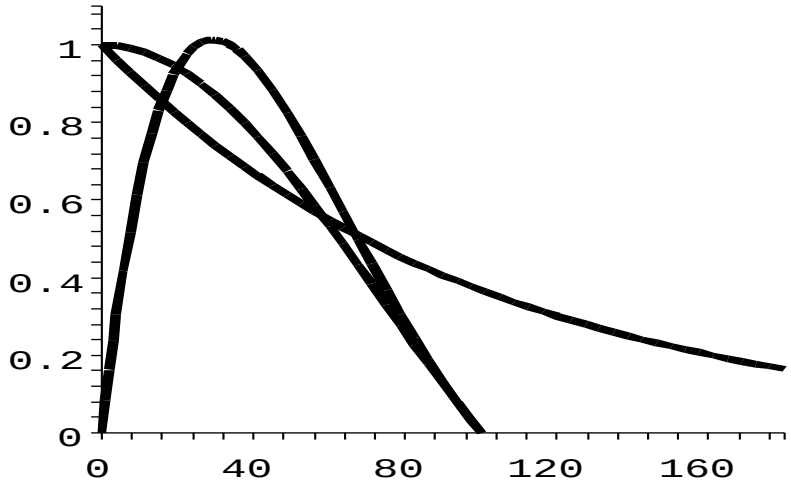

Figure 5: The special solutions (8), (16) and (19) in the cases $C_2 = 0$. Parameter values: $b = 1$ in all cases; $a = 2$ for Cases I and II, $a = 10^{-2}$ for Case IV; $k = 10^{-4}$ for Cases III and IV, $k = 0.02$ for Case I; in each case the constant C is chosen to give a maximum concentration of approximately unity. The non-monotone curve corresponds to Case I, Case III is the other curve which has zero concentration at $r = 100$, and the exponentially decaying curve corresponds to Case IV.

3 Porous medium model of a growing biofilm

3.1 Introduction

In this section we present a model of a growing biofilm, find its growth rate, and investigate the development of spatial inhomogeneities at its surface. It has been observed that if a biofilm grows in the presence of a shear flow at its surface then its shape depends on the shear rate. If the flow is slow then mushroom-like structures will develop at the biofilm surface. With a fast flow the surface of the biofilm is approximately flat. We hypothesize that the mechanism for the mushroom development may be as follows: if there is a region of the biofilm surface that is higher than the surrounding area, then this region will receive more nutrient as it is closer to the bulk flow supplying the nutrients. In turn this leads to a faster cell-division rate in the region, and hence the biofilm grows even taller in that region when compared to the surrounding area, which is also growing, but at a slower rate. If the bulk flow is faster then the nutrients are better mixed over the biofilm surface, leading to a more even growth rate.

To investigate the effect of the flow rate over the biofilm on the shape of the biofilm, we develop and analyse a two-dimensional model of a growing biofilm. We follow the model of [11] by treating treat the biofilm as a porous solid, and we assume that the growth rate is controlled by a single substrate, which diffuses through the biofilm. Far from the biofilm the flow is constant and parallel to the substratum and the substrate concentration is constant. A diagram indicating the main features of the model is shown in figure 6.

We assume that the substratum on which the biofilm develops is at $z^* = 0$ (stars denote dimensional variables), and that the biofilm occupies the region $0 < z^* < h^*(x^*, t^*)$. We treat the biofilm as a porous solid filled with incompressible fluid of viscosity μ^*, Darcy velocity $\mathbf{u}_b^*$ and pressure p_b^*, and assume that within the biofilm the bacterial cells and EPS matrix occupy

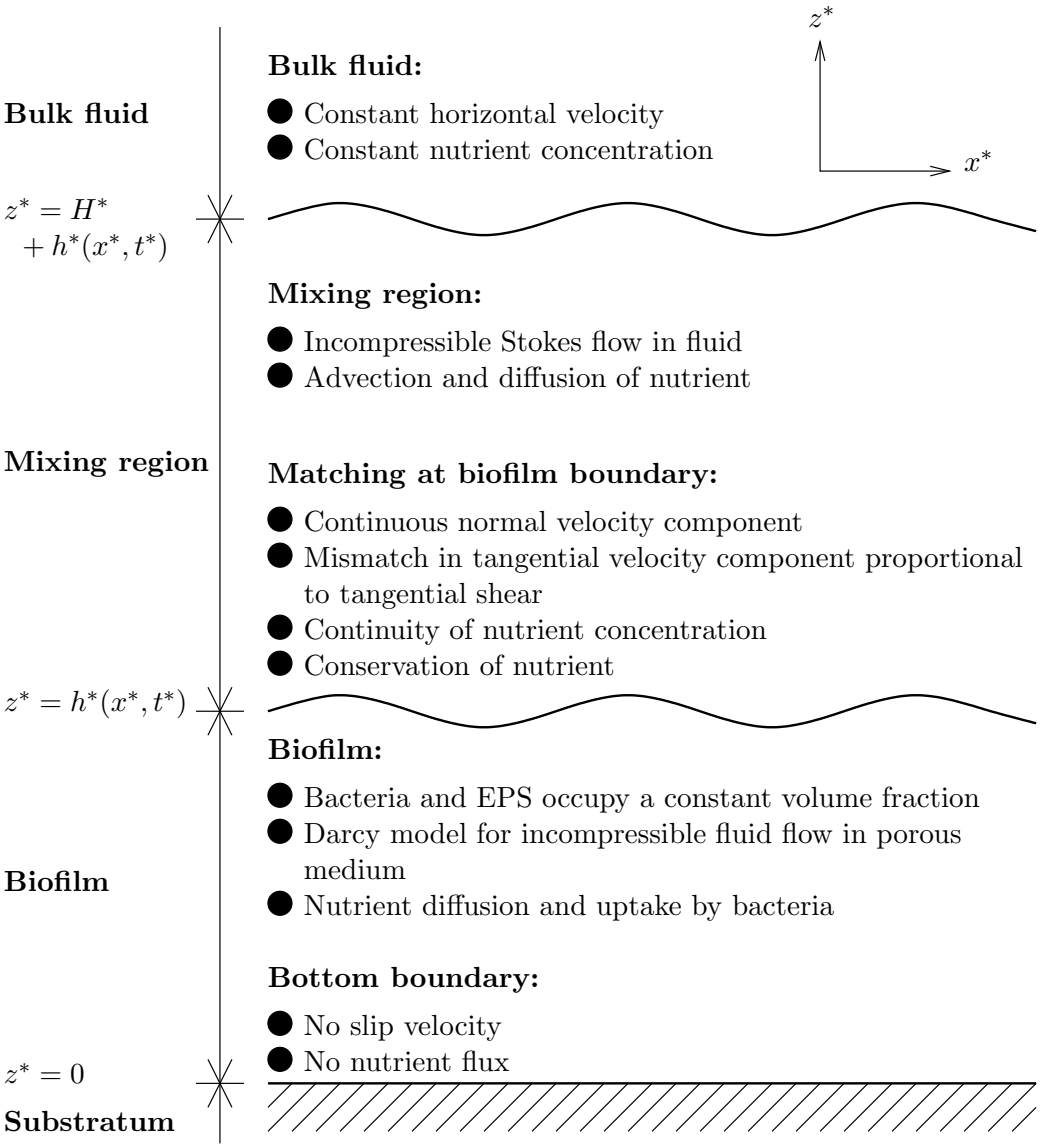

Figure 6: Model set up

a constant volume fraction, β. Thus the actual fluid velocity in the pores is $\mathbf{u}_b^*/(1-\beta)$, and, using the Darcy model, we obtain

$$\mathbf{u}_b^* = -(k^*/\mu^*)\boldsymbol{\nabla}^* p_b^*, \tag{23}$$

$$\boldsymbol{\nabla}^* \cdot \mathbf{u}_b^* = 0, \tag{24}$$

where k^* is the permeability of the biofilm. We assume that the cells consume nutrient at a rate proportional to the amount of nutrient available (this is true only for small nutrient concentrations). The nutrient is also diffused and advected within the biofilm, so

$$(1-\beta)D^*\nabla^{*2}c_b^* = \mathbf{u}_b^* \cdot \boldsymbol{\nabla}^* c_b^* + \beta(1-\beta)f^* c_b^*, \tag{25}$$

where c_b^* is the nutrient concentration in the fluid contained in the pores of the biofilm, D^* is the diffusion constant and f^* is a constant measuring the nutrient consumption rate, and depends on the species of bacteria. At $z^* = 0$ we assume no flux of nutrient into the substratum, so $\partial c_b^*/\partial z^* = 0$, and that there is no flow into the substratum, so $w^* = 0$.

Above the biofilm we consider a mixing region filled with the fluid, in which we assume that the flow, with velocity $\mathbf{u}_f^*$ and pressure p_f^*, is sufficiently slow that we may neglect inertial terms, and thus

$$\boldsymbol{\nabla}^* p_f^* = \mu^* \nabla^{*2} u_f^* \tag{26}$$

and

$$\boldsymbol{\nabla}^* \cdot \mathbf{u}_f^* = 0. \tag{27}$$

The substrate is advected and diffused through this layer, so

$$\mathbf{u}_f^* \cdot \boldsymbol{\nabla}^* c_f^* = D^* \nabla^{*2} c_f^*, \tag{28}$$

where c_f^* is the concentration of substrate. In the bulk fluid far from the biofilm, we assume there is a constant flow with constant velocity, u_0^*, in the x-direction and substrate concentration, c_0^*. We assume that this persists for $z^* > h^* + H^*$, where H^* is some arbitrarily chosen height, which provides us with boundary conditions at the top of the mixing region.

At the boundary of the biofilm mass conservation implies $\mathbf{n} \cdot \mathbf{u}_f^* = \mathbf{n} \cdot \mathbf{u}_b^*$, where $\mathbf{n}$ is a unit vector normal to the surface. In the tangential direction, we assume that the difference in tangential velocities across the interface is proportional to the shear stress, so that

$$\mathbf{t} \cdot (\mathbf{u}_f^* - \alpha^* \mathbf{n} \cdot \boldsymbol{\nabla}^* \mathbf{u}_f^*) = \mathbf{t} \cdot \mathbf{u}_b^*, \tag{29}$$

where α^* is constant proportional to $\sqrt{k^*}$ [4]. We also apply continuity of the nutrient concentration, and conservation of the nutrient itself, meaning that $c_f^* = c_b^*$ and $D^* \mathbf{n} \cdot \boldsymbol{\nabla}^* c_f^* - \mathbf{n} \cdot \mathbf{u}_f^* c_f^* = (1-\beta) D^* \mathbf{n} \cdot \boldsymbol{\nabla}^* c_b^* - \mathbf{n} \cdot \mathbf{u}_b^* c_b^*$ at the boundary of the biofilm.

Finally, we assume that the rate of cell division is proportional to nutrient uptake, and that the cells maintain a constant volume fraction of the biofilm as they divide. Thus

$$\frac{\partial h^*}{\partial t^*} = g^* \int_0^{h^*} \beta(1-\beta) f^* c^* \, dz^*,$$

for some constant g^*. Table 1 shows typical values of the parameters to be used in the model.

Parameter	**Description**	**Value**
D^*	Diffusion coefficient of oxygen in water at 20° C	$2.0 \times 10^{-9}\,\mathrm{m}^2\,\mathrm{s}{-1}$
μ^*	Viscosity of water at 20° C	$1.002 \times 10^{-3}\,\mathrm{kg\,m^{-1}\,s^{-1}}$
β	Volume fraction of bacteria	0.6
u_0^*	Flow speed in bulk	$4 \times 10^{-4}\,\mathrm{m\,s^{-1}}$
f^*	Rate of oxygen consumption by bacteria	0.2 – $1.1\,\mathrm{s^{-1}}$ [20]
h^*	Height of well-developed biofilm	$7 \times 10^{-5}\,\mathrm{m}$
c_0^*	Concentration of oxygen in the bulk	$10^{-3}\,\mathrm{kg\,m^{-3}}$
r^*	Maximum cell division rate	$10^{-4}\,\mathrm{s^{-1}}$

Table 1: Typical values of dimensional parameters.

3.2 Nondimensionalisation of model equations

We nondimensionalise lengths with respect to H^*, times with respect to H^*/u_0^*, velocities with respect to u_0^*, pressures with respect to $\mu^* u_0^*/H^*$, and concentrations with respect to c_0^*. Thus

$$x^* = H^* x, \quad z^* = H^* z, \quad h^* = H^* h, \quad t^* = \frac{H^*}{u_0^*} t,$$

$$u_i^* = u_0^* u_i, \quad w_i^* = u_0^* w_i, \quad p_i^* = \frac{\mu^* u_0^*}{H^*} p_i, \quad c_i^* = c_0^* c_i.$$

where i is either b or f. Letting

$$D = \frac{D^*}{H^* u_0^*}, \quad k = \frac{k^*}{H^{*2}}, \quad f = \frac{H^* \beta (1-\beta) f^*}{u_0^*}, \quad \alpha = \frac{\alpha^*}{H^*}, \quad g = \frac{H^* \beta (1-\beta) c_0^* f^* g^*}{u_0^*},$$

we obtain the governing equations

$$\mathbf{u}_b = -k \boldsymbol{\nabla} p_b, \quad \boldsymbol{\nabla} \cdot \mathbf{u}_b = 0, \quad (1-\beta) D \nabla^2 c_b = \mathbf{u}_b \cdot \boldsymbol{\nabla} c_b + f c_b, \tag{30}$$

$$\nabla^2 \mathbf{u}_f = \boldsymbol{\nabla} p_f, \quad \boldsymbol{\nabla} \cdot \mathbf{u}_f = 0, \quad D \nabla^2 c_f = \mathbf{u}_f \cdot \boldsymbol{\nabla} c_f. \tag{31}$$

These are to be solved subject to the boundary conditions $u_b = w_b = \partial c_b / \partial z = 0$ at $z = 0$ and $u_f = 1$, $w_f = 0$, $c_f = 1$ at $z = h + 1$. At the biofilm boundary, $z = h$, we require the matching conditions

$$\mathbf{n} \cdot \mathbf{u}_f = \mathbf{n} \cdot \mathbf{u}_b, \quad \mathbf{t} \cdot (\mathbf{u}_f - \alpha \mathbf{n} \cdot \boldsymbol{\nabla} \mathbf{u}_f) = \mathbf{t} \cdot \mathbf{u}_b,$$

$$c_f = c_b, \quad \mathbf{n} \cdot (D \boldsymbol{\nabla} c_f - \mathbf{u}_f c_f) = \mathbf{n} \cdot \left((1-\beta) D \boldsymbol{\nabla} c_b - \mathbf{u}_b c_b \right), \tag{32}$$

where $\mathbf{n}$ and $\mathbf{t}$ are unit vectors normal and tangential to the biofilm surface respectively. The biofilm growth rate is now given by

$$\frac{\partial h}{\partial t} = g \int_0^h c \, dz. \tag{33}$$

3.3 Basic state

Equations (30) and (31) admit an x-independent solution as follows:

$$u_b = w_b = 0, \quad c_b = \frac{\cosh \gamma z}{\cosh \gamma h + \gamma (1-\beta) \sinh \gamma h}, \tag{34}$$

$$u_f = \frac{z + \alpha - h}{1 + \alpha}, \quad w_f = 0, \quad c_f = \frac{\cosh \gamma h + \gamma (1-\beta)(z-h) \sinh \gamma h}{\cosh \gamma h + \gamma (1-\beta) \sinh \gamma h}, \tag{35}$$

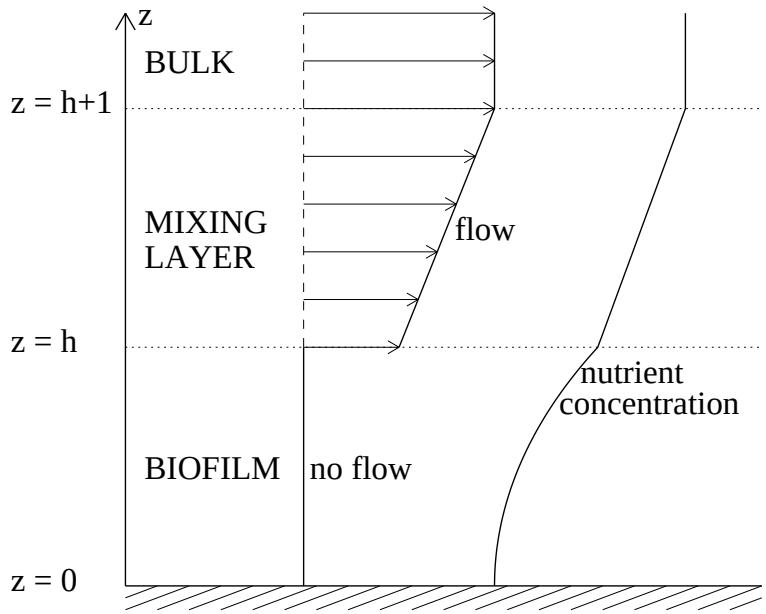

Figure 7: Sketch graphs of the flow rate and nutrient concentration in the x-independent state of the biofilm.

where $\gamma = \sqrt{f/(1-\beta)D}$. Sketch graphs of this solution are shown in figure 7. The velocity is horizontal and has a linear shear in the mixing region and no flow in the biofilm. The concentration profile follows a linear profile in the mixing region, and decreases more slowly within the biofilm. The growth rate of the biofilm is given by the solution of

$$\frac{\partial h}{\partial t} = \frac{g}{\gamma}\left(\frac{\sinh\gamma h}{\cosh\gamma h + \gamma(1-\beta)\sinh\gamma h}\right). \tag{36}$$

Thus if $h \ll \gamma^{-1}$ the biofilm grows approximately exponentially according to $h \approx h_0 e^{gt}$ for some constant h_0. For larger heights $h \gg \gamma^{-1}$ there is linear growth according to $h \approx \tilde{h}_0 + gt/(\gamma(1+(1-\beta)\gamma))$ where $\tilde{h}_0$ is constant. Using the parameter values in table 1 and H^* equal to a typical biofilm height, *i.e.* $70\,\mu$m, gives $\gamma \approx 0.54$, and to estimate g we assume that the nutrient concentration in the bulk, c_0^*, is just sufficient to enable the cells to divide at their maximum rate. This gives $g = H^* r^*/u_0^*$, where r^* is the maximum division rate, which is approximately 1.75×10^{-5} for the given parameter values. Note that the value of γ is independent of the flow rate, u_0^*, and thus the flow only affects the value of dh^*/dt^* through the value of g, which is proportional to $1/u_0^*$. Graphs of the growth rate are shown in figure 8 for various values of γ, which show approximately exponential growth for small values of h and linear growth for large h.

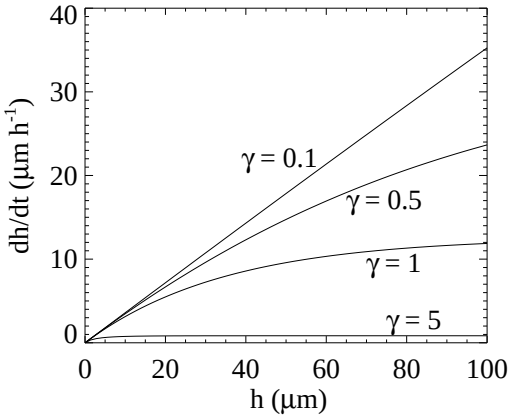

Figure 8: Graph showing the growth rate of the biofilm against height of biofilm for various values of γ with $g = 1.75 \times 10^{-5}$.

3.4 Perturbations to the basic state

We now find the stability of this solution to a small perturbation of height $\epsilon e^{\mathrm{i}\lambda x} + \text{c.c.}$, where $\lambda \in \mathbb{C}$, c.c. denotes the complex conjugate and $\epsilon \ll 1$. We seek a solution of the form

$$h = h_0 + \epsilon(e^{\mathrm{i}\lambda x} + \text{c.c.}),$$
$$u_b = \epsilon(u_{b1}e^{\mathrm{i}\lambda x} + \text{c.c.}), \quad w_b = \epsilon(w_{b1}e^{\mathrm{i}\lambda x} + \text{c.c.}), \quad c_b = c_{b0} + \epsilon(c_{b1}e^{\mathrm{i}\lambda x} + \text{c.c.}),$$
$$u_f = u_{f0} + \epsilon(u_{f1}e^{\mathrm{i}\lambda x} + \text{c.c.}), \quad w_f = \epsilon(w_{f1}e^{\mathrm{i}\lambda x} + \text{c.c.}), \quad c_f = c_{f0} + \epsilon(c_{f1}e^{\mathrm{i}\lambda x} + \text{c.c.}),$$

where h_0, c_{b0}, u_{f0} and c_{f0} are the basic state solutions, given in (34)–(35), with h replaced by h_0, and u_{b1}, w_{b1}, c_{b1}, u_{f1}, w_{f1} and c_{f1} are functions of z and t only.

The equations (30)–(31) give rise to the following system at $\mathcal{O}(\epsilon)$:

$$\frac{\partial u_{b1}}{\partial z} - \mathrm{i}\lambda w_{b1} = 0, \quad \mathrm{i}\lambda u_{b1} + \frac{\partial w_{b1}}{\partial z} = 0, \quad (1-\beta)D\left(\frac{\partial^2 c_{b1}}{\partial z^2} - \lambda^2 c_{b1}\right) = \frac{\partial c_{b0}}{\partial z} w_{b1} + f c_{b1}, \quad (37)$$

$$\frac{\partial}{\partial z}\left(\frac{\partial^2 u_{f1}}{\partial z^2} - \lambda^2 u_{f1}\right) - \mathrm{i}\lambda\left(\frac{\partial^2 w_{f1}}{\partial z^2} - \lambda^2 w_{f1}\right) = 0, \quad \mathrm{i}\lambda u_{f1} + \frac{\partial w_{f1}}{\partial z} = 0,$$
$$D\left(\frac{\partial^2 c_{f1}}{\partial z^2} - \lambda^2 c_{f1}\right) = \mathrm{i}\lambda u_{f0} c_{f1} + \frac{\partial c_{f0}}{\partial z} w_{f1}. \quad (38)$$

At $z = 0$ the boundary conditions are $u_{b1} = w_{b1} = \partial c_{b1}/\partial z = 0$, and at $z = 1 + h$

$$u_{f0} + \epsilon\left(u_{f1}e^{\mathrm{i}\lambda x} + \text{c.c.}\right) = \epsilon\left(w_{f1}e^{\mathrm{i}\lambda x} + \text{c.c.}\right) = c_{f0} + \epsilon\left(c_{f1}e^{\mathrm{i}\lambda x} + \text{c.c.}\right) = 0,$$

which gives the boundary conditions at $\mathcal{O}(\epsilon)$

$$\frac{\partial u_{f0}}{\partial z} + u_{f1} = w_{f1} = \frac{\partial c_{f0}}{\partial z} + c_{f1} = 0, \quad (39)$$

at $z = 1 + h_0$. To apply the matching conditions at $z = h$ we note that $\mathbf{t} = (1, \epsilon(\mathrm{i}\lambda e^{\mathrm{i}\lambda x} +$

c.c.)) + $\mathcal{O}(\epsilon^2)$ and $\mathbf{n} = (-\epsilon(\mathrm{i}\lambda e^{\mathrm{i}\lambda x} + \text{c.c.}), 1) + \mathcal{O}(\epsilon^2)$, and the conditions (32) become

$$\begin{aligned}
\epsilon\left((-\mathrm{i}\lambda u_{f0} + w_{f1})e^{\mathrm{i}\lambda x} + \text{c.c.}\right) =& \epsilon\left(w_{b1}e^{\mathrm{i}\lambda x} + \text{c.c.}\right) + \mathcal{O}(\epsilon^2),\\
u_{f0} - \alpha\frac{\partial u_{f0}}{\partial z} + \epsilon\left((u_{f1} - \alpha\frac{\partial u_{f1}}{\partial z})e^{\mathrm{i}\lambda x} + \text{c.c.}\right) =& \epsilon\left(u_{b1}e^{\mathrm{i}\lambda x} + \text{c.c.}\right) + \mathcal{O}(\epsilon^2),\\
c_{f0} + \epsilon\left(c_{f1}e^{\mathrm{i}\lambda x} + \text{c.c.}\right) =& c_{b0} + \epsilon\left(c_{b1}e^{\mathrm{i}\lambda x} + \text{c.c.}\right),\\
D\frac{\partial c_{f0}}{\partial z} + \epsilon\left(\left(\mathrm{i}\lambda u_{f0}c_{f0} + D\frac{\partial c_{f1}}{\partial z} - c_{f0}w_{f1}\right)e^{\mathrm{i}\lambda x} + \text{c.c.}\right) =& (1-\beta)D\frac{\partial c_{b0}}{\partial z}\\
&+ \epsilon\left(\left((1-\beta)D\frac{\partial c_{b1}}{\partial z} - c_{b0}w_{b1}\right)e^{\mathrm{i}\lambda x} + \text{c.c.}\right) + \mathcal{O}(\epsilon^2),
\end{aligned}$$

and at $\mathcal{O}(\epsilon)$ this gives the matching conditions

$$-\mathrm{i}\lambda u_{f0} + w_{f1} = w_{b1}, \tag{40}$$

$$\frac{\partial u_{f0}}{\partial z} - \alpha\frac{\partial^2 u_{f0}}{\partial z^2} + u_{f1} - \alpha\frac{\partial u_{f1}}{\partial z} = u_{b1}, \tag{41}$$

$$\frac{\partial c_{f0}}{\partial z} + c_{f1} = \frac{\partial c_{b0}}{\partial z} + c_{b1}, \tag{42}$$

$$D\frac{\partial^2 c_{f0}}{\partial z^2} + \mathrm{i}\lambda u_{f0}c_{f0} + D\frac{\partial c_{f1}}{\partial z} - c_{f0}w_{f1} = (1-\beta)D\frac{\partial^2 c_{b0}}{\partial z^2} + (1-\beta)D\frac{\partial c_{b1}}{\partial z} - c_{b0}w_{b1}, \tag{43}$$

at $z = h_0$.

From the $\mathcal{O}(\epsilon)$ contributions to equation (33) we may now calculate the growth rate of the perturbation in h, which is governed by

$$\frac{\partial \epsilon}{\partial t} = G\epsilon,$$

to $\mathcal{O}(\epsilon)$, where the growth rate,

$$G = g\left(c_{b0}|_{z=h_0} + \int_0^{h_0} c_{b1}\,dz\right).$$

Solving (37a) and (37b) and applying the bottom boundary condition gives no flow in the biofilm, *i.e.* $u_{b1} = w_{b1} = 0$. The equation (37c) together with the bottom boundary condition gives

$$c_{b1} = C\cosh(\sqrt{\gamma^2 + \lambda^2}z),$$

where C must be determined by matching to the concentration profile in the mixing layer, and thus

$$G = g\left(\frac{\cosh\gamma h_0}{\cosh\gamma h_0 + \gamma(1-\beta)\sinh\gamma h_0} + \frac{C\sinh(\sqrt{\gamma^2+\lambda^2}h_0)}{\sqrt{\gamma^2+\lambda^2}}.\right) \tag{44}$$

Equations (38a) and (38b) have solution

$$\begin{aligned}
w_{f1} =& (A_1 + A_2 z)\,e^{-\lambda z} + (A_3 + A_4 z)\,e^{\lambda z},\\
u_{f1} =& \mathrm{i}\left(-A_1 - A_2 z + \frac{A_2}{\lambda}\right)e^{-\lambda z} + \mathrm{i}\left(A_3 + A_4 z + \frac{A_4}{\lambda}\right)e^{\lambda z},
\end{aligned}$$

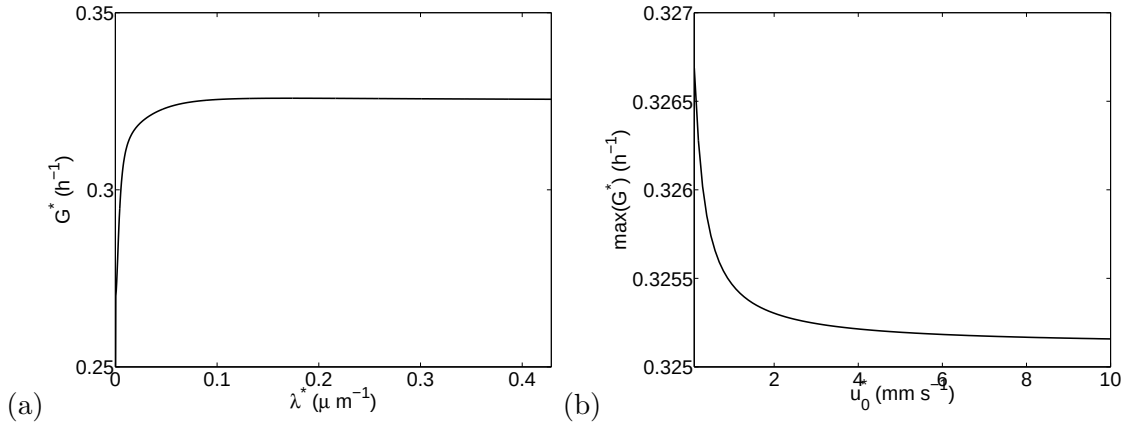

Figure 9: (a) Growth rate of perturbation as a function of its wavenumber using $u_0^* = 4 \times 10^{-4}\,\mathrm{m\,s^{-1}}$. (b) Graph showing the maximum growth rate over λ against the bulk flow rate. For both these graphs we used $\beta = 0.6$, $h_0 = 1$, $\alpha = 1$, $D = 0.071$, $\gamma = 0.54$, $g = 1.75 \times 10^{-5}$, $\lambda^* = \lambda/H^*$ and $G^* = Gu_0^*/H^*$.

where the constants A_i may be determined by applying the boundary conditions (39), (40) and (41). Finally c_{f1} satisfies the linear second order ODE

$$D\frac{\partial^2 c_{f1}}{\partial z^2} - \left(D\lambda^2 + \mathrm{i}\lambda\frac{z+\alpha-h_0}{1+\alpha}\right)c_{f1} = \frac{\gamma(1-\beta)\sinh(\gamma h_0)}{\cosh(\gamma h_0)+\gamma(1-\beta)\sinh(\gamma h_0)}\left((A_1+A_2 z)e^{-\lambda z} + (A_3+A_4 z)e^{\lambda z}\right) \quad (45)$$

together with the boundary conditions

$$\frac{\partial c_{f1}}{\partial z} - (1-\beta)\sqrt{\gamma^2+\lambda^2}\tanh\left(\sqrt{\gamma^2+\lambda^2}h_0\right)c_{f1} = \frac{(1-\beta)\gamma^2\cosh(\gamma h_0) - \gamma\beta(1-\beta)\sqrt{\gamma^2+\beta^2}\tanh(\sqrt{\gamma^2+\lambda^2}h_0)\sinh(\gamma h_0)}{\cosh(\gamma h_0)+\gamma(1-\beta)\sinh(\gamma h_0)} \quad \text{at } z = h_0,$$

$$c_{f1} = -\frac{\gamma(1-\beta)\sinh(\gamma h_0)}{\cosh(\gamma h_0)+\gamma(1-\beta)\sinh(\gamma h_0)} \quad \text{at } z = 1+h_0.$$

Solving equation (45) yields the value of C, which in turn enables the growth rate to be found from equation (44).

3.5 Discussion

We solve equation (45) numerically to find the growth rate of the biofilm. The parameter values provided in table 1 give $D \approx 0.071$ and $\gamma \approx 0.54$, and as before we approximate g by $H^* r^*/u_0^* \approx 1.75 \times 10^{-5}$. The value of α was not found to affect the growth rates significantly; for convenience we set $\alpha = 1$. Note that the permeability, k, does not affect the growth rate.

A graph of the biofilm growth rate against the wavenumber, λ, is shown in figure 9(a). The growth rate is everywhere positive, indicating that the flat state is unstable to perturbation of any wavelength. The growth rate attains its minimum value at $\lambda^* = 0$, and increases to a finite maximum before slowly decreasing as λ^* increases further. Once the flat state is perturbed the instability will continue to grow until our assumption that $\epsilon \ll 1$ is no longer valid. After

this the evolution will be determined by the nonlinear terms that we neglected in the above analysis. Finding the exact structure would involve solving the equations (30) and (31) in two dimensions, which is beyond the scope of this report.

The graphs in figure 9(b) show that the maximum growth rate of the perturbations decreases slightly as u_0^* increases. This may indicate that the biofilm surface could be more uneven if the flow rate is slow, which would agree with observations and with our hypothesis.

4 The effects of flow and nutrient transport on biofilm morphology

We construct a model of biofilm formation by modifying Mimura,-Sakaguchi- Matsushita's bacterial colony model (MSM model) [17]. MSM model is originally designed for reproducing the various pattens of bacterial colonies on the agar plate. Thus, it is a 2 dimensional model defined on x-y plane (horizontal plane). Here we regard this model as defined on x-z plane (vertical plane). It is straight forward to extend it to a 3 dimensional model, although it is not shown in this report. Our model includes 3 variables c, u and v.

c : concentration of nutrient

u : concentration of active bacteria in biofilms

v : concentration of dormant bacteria (plus EPS)

The model equations are

$$\begin{aligned}
\frac{\partial c}{\partial t} &= \nabla \cdot (D_c(v)\nabla c) - \alpha c u + r(v) f(z)(\bar{c} - c), \\
\frac{\partial u}{\partial t} &= \nabla \cdot (D_u(v)\nabla u) + cu - \beta(c) u, \\
\frac{\partial v}{\partial t} &= \beta(c) u,
\end{aligned}$$

where the functions $D_c(v)$, $D_u(v)$ and $r(v)$ are of similar form such as ae^{-bv} (a, b : positive constant). The function $\beta(c)$ gives the conversion rate from active bacteria to dormant bacteria, which includes the switching mechanism controlled by the concentration of nutrient.

The last term of the right hand side of the first equation indicates a supply of nutrient by the fluid flow ($\bar{c}$ is a concentration of the nutrient in the upwind region). In the absence of this term, this equation simply gives a description of the diffusion limited growth which is quite similar to the phase field model of diffusion limited crystal growth. Therefore, a cellular growth pattern is expected, which implies the formation of pillar structure in this case.

Because the flow rate is larger in the distant area from the substrate, the situation there is less "diffusion limited" than the neighbour of the substrate. The function $f(z)$ gives a phenomenological evaluation of the influence of flow, which is increasing and $f(0) = 0$. Under the existence of nutrient supply by flow, the pillars become fat as they grows, finally they merge together.

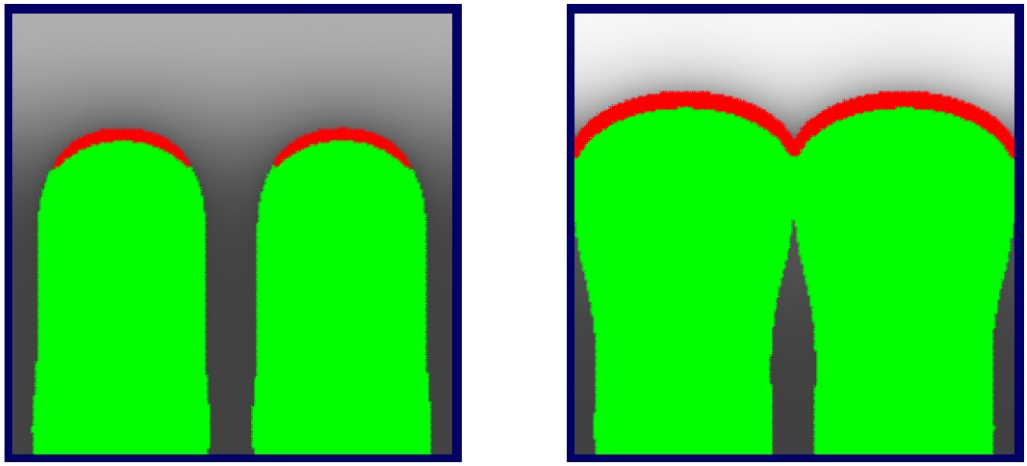

Figure 10: The left panel shows a pillar structure which is obtained by the simulation without fluid flow, while the right panel presents merged pillars induced by the influence of the fluid flow. Red region (or, in black and white, dark grey region on top of the pillar) is a u-rich region, green region (the pale grey pillars) is a v-rich region, and grey level (grey shades above and between pillars) indicates the level of w.

5 Modelling the role of quorum sensing in biofilm detachment

5.1 Introduction

The structure of biofilms, at least in an experimental set up, broadly consists of bacteria (living and dead), exo-polysaccharide (or EPS, a matrix structure that provides structural integrity to the biofilm) and water. Within the biofilm, individual bacteria are usually sessile, lacking a flagellum (so they cannot swim) and are held fast by the EPS structure. In mature biofilms, cells on the surface can become planktonic enabling them to escape and swim in the surrounding media, enabling the bacteria to colonise new sites. What triggers this change of phenotype on surface bacteria seems to depend on the species. It is probable, that the detachment process is one of the main reasons why biofilms seem to grow to a maximal depth.

For *Rhodobacter sphaeroides* the expression of the planktonic phenotype may be regulated by a cell-cell signalling process called quorum sensing (QS). In brief, QS involves the release into the environment of a diffusible molecule (AHL, sometimes called an autoinducer), which can form a complex with a cognate protein, sited within the bacteria's cytoplasm, which can then bind to a site on the DNA (called the *lux*-box). An occupied *lux*-box enables the expression of a number of genes down-stream along the DNA, up-regulating the production of a number of enzymes and proteins that enhances significantly the production rate of AHLs (hence the monicker autoinducer) and induce changes in the bacteria's phenotypes; these enzymes and proteins will not be produced if the *lux*-box is empty. In *R. sphaeroides*, up-regulation through QS has the effect of reducing their propensity to aggregate, enabling planktonic cells to disperse from a biofilm; strains lacking a functioning QS apparatus form non-motile sticky clumps [21]. In practice, a bacterial colony with a small population density will be in the "down-regulated mode" and at high density the cells will be predominantly "up-regulated"; as the population increases density, the transition from a "down-regulated" population to one which is "up-regulated" tends to be very rapid in comparison to the rate of

population growth.

In biofilms, AHLs will be lost to the outside media via diffusion through the surface and they will therefore accumulate most in the inner regions. For *R. sphaeroides*, this would suggest that the inner cells will be switching to the planktonic form, however, this would be a waste of energy as the EPS will prevent them from swimming anywhere. This would suggest that signals other than QS are needed to trigger planktonic activation in *R. sphaeroides*, basically something to tell the bacteria whether they are close to the surface or not. In the modelling below, we investigate the role of nutrient as a possible secondary regulating signal. The issues to be investigated are

- The role of quorum sensing and nutrients in bacterial escape from the biofilm.
- Whether detachment through phenotypic change to planktonic cells can limit the biofilm depth as seems to be observed in experiments.

5.2 Mathematical modelling

For simplicity, the model will be one-dimensional, in which the biofilm is defined to be in the region $0 \leq z \leq h(t)$, where $z = h(t)$ is the moving coordinate of the biofilm surface (see Figure 11).

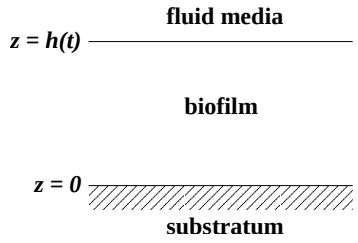

Figure 11: Schematics of the 1-D depth based biofilm model.

The biofilm consists of bacteria, water and EPS. Again, for simplicity, we will assume that the volume fraction of bacteria within the biofilm will be kept constant,[2] namely ϕ ($\phi \in (0, 1]$). The bacteria consists of three sub-populations:

$n(z,t)$: volume fraction of down-regulated bacteria,
$q(z,t)$: volume fraction of up-regulated, but non-planktonic, bacteria,
$p(z,t)$: volume fraction of up-regulation and planktonic bacteria,

such that

$$n + q + p = \phi. \tag{46}$$

The transitions between sub-populations is dependent on the AHL concentration, a. AHLs are produced by all cells, but at a significantly low rate by the down-regulated bacteria. Up-regulated cells can spontaneously down-regulate, reflecting decomposition of the *lux*-box bound complex; planktonic individuals are assumed to lose the flagellum when this occurs. These assumptions are based on an earlier work [25]. Non-planktonic cells require nutrients

[2]The timescale for change of phenotype is 10 minutes, whereas the timescale for division is every hour, so this is not unreasonable as a first approximation.

(concentration c) to become planktonic and the reverse process occurs spontaneously. Bacterial growth and cell division is governed by the concentration of nutrients, which is assumed to be fixed in the fluid media and diffuses into the biofilm and is consumed by the bacteria. This growth generates cell movement described by the advective velocity v. Assuming on the timescale of interest (bacterial doubling time, i.e. about an hour), the diffusion rates of c and a far exceed that of transport via advection, the model is thus

$$\frac{\partial n}{\partial t} + \frac{\partial (vn)}{\partial z} = f_b(c)\,(n + (2-\gamma)q + (2-\gamma)p) \; - \; \alpha a n \; + \; \beta(q+p), \tag{47}$$

$$\frac{\partial q}{\partial t} + \frac{\partial (vq)}{\partial z} = (\gamma - 1) f_b(c)\, q \; - \; f_p(c) q \; + \alpha a n \; - \; \beta q \; + \; \delta p, \tag{48}$$

$$\frac{\partial p}{\partial t} + \frac{\partial (vp)}{\partial z} = (\gamma - 1) f_b(c)\, p \; + \; f_p(c) q \; - \; \delta p \; - \; \beta p, \tag{49}$$

$$0 = D_a \frac{\partial^2 a}{\partial z^2} \; + \; \kappa_u (p+q) \; + \; \kappa_n \, n \; - \; \alpha a n \; - \; \lambda a, \tag{50}$$

$$0 = D_c \frac{\partial^2 c}{\partial z^2} \; - \; \phi f_c(c), \tag{51}$$

$$\frac{\partial v}{\partial z} = f_b(c), \tag{52}$$

where (52) was derived from summing (47)-(49) using (46). The exact functional forms of $f_b(c)$ and $f_p(c)$ are not known, although we expect both to be monotonically increasing in c. In the simulations to follow we used $f_b(c) = f_{b0} c$ and $f_p(c) = f_{p0} c^m / (c_p^m + c^m)$, where the latter function is chosen to ensure the switching to planktonic state occurs near the surface. The constant γ (where $\gamma \in [0, 2]$) in the birth rate terms is the average number of occupied *lux*-boxes on the two chromosomes following cell-division of up-regulated cells; $\gamma = 1$ represents one occupied and one empty *lux*-box (which, for simplicity, will be henceforth adopted), whilst $\gamma = 0$ implies the complex on the occupied *lux*-box is broken-down during the replication process. The nutrient and AHL molecules are assume to diffuse freely across the bacterial membrane. The initial and boundary conditions are

$$\begin{aligned} t = 0 \qquad & n = \phi, \; p = 0, \; q = 0, \; h = H_0 \\ z = 0 \qquad & \frac{\partial c}{\partial z} = \frac{\partial a}{\partial z} = v = 0, \\ z = h(t) \qquad & \frac{dh}{dt} = v - \sigma p, \; D_a \frac{\partial a}{\partial z} = -Qa, \; c = c_0. \end{aligned}$$

The initial population is assumed to consist of entirely down-regulated cells and the rate of biofilm growth is equal to the surface velocity minus the volume lost through cell detachment.

5.2.1 Non-dimensionalisation

We write

$$t = \frac{\hat{t}}{f_{b0} c_0}, \; z = H_0 \, \hat{z}, \; c = c_0 \, \hat{c}, \; a = \frac{\kappa_u H_0^2}{D_a} \, \hat{a}, \; v = H_0 f_{b0} c_0 \, \hat{v}, \; h = H_0 \, \hat{h}$$

$$\varepsilon = \frac{\kappa_n}{\kappa_u}, \; \hat{\alpha} = \frac{\alpha \kappa_u H_0^2}{D_a f_{b0} c_0}, \; \hat{\beta} = \frac{\beta}{f_{b0} c_0}, \; \hat{\delta} = \frac{\delta}{f_{b0} c_0}, \; \mu = \frac{\alpha H_0^2}{D_a}, \; \hat{\lambda} = \frac{\lambda H_0^2}{D_a},$$

$$\hat{c}_p = c_p / c_0, \; \eta = \frac{f_{p0}}{f_{b0} c_0} \left(1 + \frac{c_p^m}{c_0^m} \right), \; \rho = \frac{f_{c0} H_0^2}{D_c}, \; \hat{\sigma} = \frac{\sigma}{H_0 f_{b0} c_0}, \hat{Q} = \frac{Q H_0}{D_a},$$

hence $\hat{f}_p(\hat{c}) = \eta(1+\hat{c}_p^m)\hat{c}^m/(\hat{c}_p^m+\hat{c}^m)$. Here time has been scaled to the maximum cell division rate $f_{b0}c_0$ (roughly an hour), depth has been scaled with the initial depth and n, q, p have remained unscaled so that the role of bacterial cell volume fraction, ϕ, on biofilm development is made explicit. These rescalings lead to, on fixing $\gamma = 1$,

$$\frac{\partial n}{\partial t} + \frac{\partial (vn)}{\partial z} = \phi c - \alpha a n + \beta(q+p), \tag{53}$$

$$\frac{\partial q}{\partial t} + \frac{\partial (vq)}{\partial z} = -f_p(c) c\, q + \alpha a n - \beta q + \delta p, \tag{54}$$

$$\frac{\partial p}{\partial t} + \frac{\partial (vp)}{\partial z} = f_p(c) c\, q - (\delta+\beta) p, \tag{55}$$

$$0 = \frac{\partial^2 a}{\partial z^2} + q + p + \varepsilon\, n - \mu a n - \lambda a, \tag{56}$$

$$0 = \frac{\partial^2 c}{\partial z^2} - \phi\rho c, \tag{57}$$

$$\frac{\partial v}{\partial z} = c, \tag{58}$$

where the hats have been dropped for clarity. We note that $n + p + q = \phi$ can be used to eliminate one of the bacterial sub-populations from the system. The dimensionless initial and boundary conditions are

$$\begin{aligned} t = 0 \qquad & p = 0,\ q = 0,\ h = 1, \\ z = 0 \qquad & \frac{\partial a}{\partial z} = \frac{\partial c}{\partial z} = v = 0, \\ z = h(t) \qquad & \frac{dh}{dt} = v - \sigma p,\ c = 1,\ \frac{\partial a}{\partial z} = -Qa. \end{aligned}$$

Solving for c and v gives

$$c = \frac{\cosh(\sqrt{\phi\rho}\, z)}{\cosh(\sqrt{\phi\rho}\, h(t))}, \tag{59}$$

$$v = \frac{\sinh(\sqrt{\phi\rho}\, z)}{\sqrt{\phi\rho}\, \cosh(\sqrt{\phi\rho}\, h(t))}, \tag{60}$$

and the biofilm will grow according to

$$\frac{dh}{dt} = \frac{1}{\sqrt{\phi\rho}} \tanh\Big(\sqrt{\phi\rho}\, h(t)\Big) - \sigma p. \tag{61}$$

We note that in the absence of planktonic cell escape ($\sigma = 0$), equation (61) is equivalent to equation 36 in Section 3, the difference being due to the presence of the mixing layer in the earlier model. For $\sigma = 0$, the biofilm will have an initial phase of accelerated growth (exponential if $\phi\rho \ll 1$), becoming linear $h \sim t/\sqrt{\phi\rho}$ as $t \to \infty$; integration gives the solution for $h(t)$

$$h(t) = \frac{1}{\sqrt{\phi\rho}} \sinh^{-1}(\sinh(\sqrt{\phi\rho})\, e^t).$$

5.3 Numerical results and analysis

The system (53)-(61) is approximated numerically using a finite-difference predictor-corrector type scheme, with the moving domain mapped to the unit interval using the translation $z = Zh(t)$. A number of simulations were performed and Figures 12 and 13 are representative.

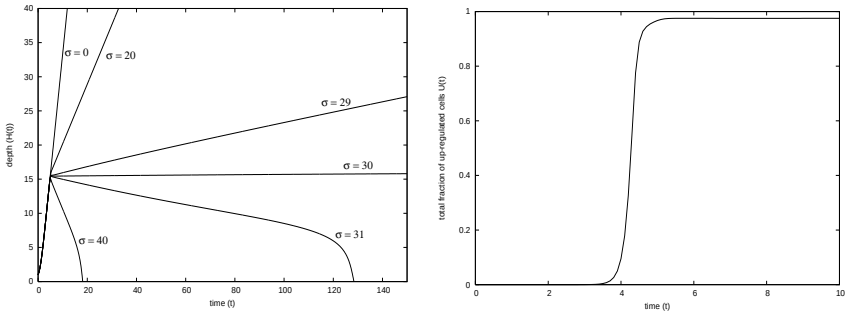

Figure 12: Plots of the biofilm depth against time for various σ (left) and total up-regulated cell fraction against time. The parameters used are $\phi = 0.8, \varepsilon = 10^{-6}, \alpha = 1, \beta = 0.2, \mu = 0.1, \lambda = 0.01, \delta = 1, \rho = 0.1, \eta = 1, c_p = 0.8, m = 4$ and $Q = 10$.

Figures 12 demonstrates the role of σ on the biofilm depth and the total up-regulated cell fraction against time. Without planktonic escape ($\sigma = 0$) the biofilm will grow linearly, and this growth is maintained as σ increases; however, there appears to be critical value ($\sigma \approx 30$) above which the planktonic escape rate far exceeds that of birth and biofilm extinction will result in finite time. This indicates the existence of a structurally unstable steady-state at the threshold value of σ; this is demonstrated in the analysis of Section 5.3.1 for a limiting case of the model. The rapid jump around $t = 4$ of the total up-regulated cell fraction $U(t)$, calculated using the formula

$$U(t) \;=\; \frac{\int_0^{H(t)} (p+q)\, dz}{\phi h(t)},$$

is characteristic of QS behaviour; where there is a delay before high QS activity occurs. It is due to this delay that the biofilm growth curves are all initially the same. Determining the timescale for substantial up-regulation is discussed in Section 5.3.2.

Figure 13 show the distribution and evolution of the main variables for a slow growth case ($\sigma = 30$). The top left plot shows the distribution of the sub-population densities in a mature biofilm. Due to the high AHL concentration and low nutrient concentration, nearly all cells are up-regulated and non-planktonic away from the surface. At the surface the nutrient concentration enables the switch to the planktonic phenotype, and with the relatively low AHL concentration the combination of spontaneous down-regulation $\beta > 0$ and cell birth means that there is also a non-negligible fraction of down-regulated cells present. The top right figure reveals a very rapid jump in AHL concentration throughout the biofilm corresponding to the time of the rapid jump in $U(t)$. The accumulation near the base of the biofilm is to be expected and the large drop towards the surface is due to the relatively large mass transport constant Q, meaning AHLs readily escape into the environment. The drop in nutrient concentration towards the base is due to consumption by the cells near the surface and the increasing velocity reflects the increasing birth rate at the surface.

5.3.1 Fully up-regulated, small-depth limit

As suggested by the numerical results above that biofilm will eventually grow linearly (as a travelling wave) or vanish in finite-time; a structurally unstable steady-state appears to lie at the bifurcation between these two outcomes. Demonstrating this analytically on the full

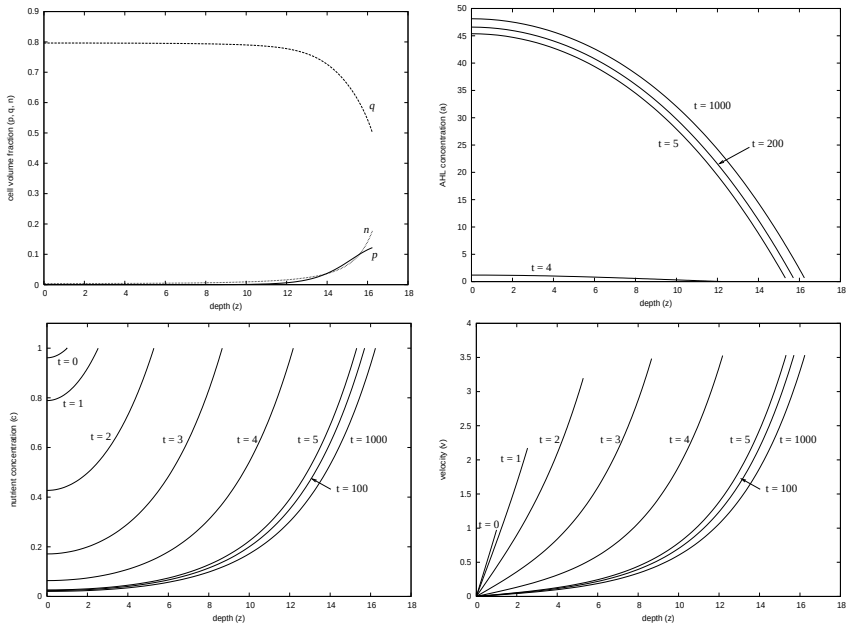

Figure 13: Plots of the sub-population distribution at $t = 1000$ (top left) and of the evolution of AHL concentration (top right), nutrient concentration (bottom left) and velocity distribution (bottom right) for the slow growth case, $\sigma = 30$, with all other parameters as given in the caption of Figure 12.

system (53)-(58) is difficult, but progress can be made when considering a near fully up-regulated biofilm with large AHL concentration ($a \gg 1$), for which the leading order balance of (53) gives

$$\alpha\, an \;\sim\; \phi c + \beta(q+p),$$

and a small depth (specifically $\phi\rho H^2 \ll 1$, so negligible nutrient is consumed), so that

$$c \;\sim 1,$$

throughout the biofilm. Since $q \sim \phi - p$ and from (58) $v \sim z$, the system reduces to

$$\frac{\partial p}{\partial t} + z\frac{\partial p}{\partial z} \;=\; \eta\,\phi \,-\, \psi p, \tag{62}$$

$$\frac{dH}{dt} \;=\; H \,-\, \sigma p(H,t), \tag{63}$$

at leading order, where $\psi = \eta+\delta+\beta+1$. Using, for generality, the initial conditions $H(0) = H_0$ and $p(z,0) = p_0(z)$, these equations have solutions

$$\begin{aligned} p &= p_\infty + (p_0(ze^{-t}) - p_\infty)e^{-\psi t}, \\ H &= (H_0 - \sigma p_\infty)e^t + \sigma p_\infty - e^t \int_0^t \left(p_0(He^{-\tau}) - p_\infty\right) e^{-(\psi+1)\tau}\, d\tau \end{aligned}$$

where $p_\infty = \phi\eta/\psi$. Since $p_0 \in [0,\phi]$ we can deduce the following bound on $H(t)$,

$$(H_0 - \sigma p_\infty)e^t + \sigma p_\infty - \frac{(\phi - p_\infty)}{\psi+1}e^{-\psi t} \;\le\; H(t) \;\le\; (H_0 - \sigma p_\infty)e^t + \sigma p_\infty + \frac{p_\infty}{\psi+1}e^{-\psi t};$$

hence, $H(t)$ will grow exponentially if $H_0 > \sigma p_\infty$ (the small-depth limit will breakdown when $\phi\rho H^2 \sim 1$) or will become zero in finite time if $H_0 < \sigma p_\infty$; $p = p_\infty$ and $H = \sigma p_\infty$ being the structurally unstable steady-state solution for this limit.

5.3.2 A sufficient condition for up-regulation in the limit $\varepsilon \to 0$

Exploiting the fact $\varepsilon \ll 1$, a sufficient condition for up-regulation in terms of the model parameters can be deduced for the case of no AHL escape to the surrounding media (i.e. $Q = 0$). For $t = O(1)$, we consider expansions of the form $p = \varepsilon p^\dagger \sim \varepsilon p_0^\dagger$, $q = \varepsilon q^\dagger \sim \varepsilon q_0^\dagger$,$c = \phi - \varepsilon n^\dagger \sim \phi - \varepsilon n_0^\dagger$ and $a = \varepsilon a^\dagger \sim \varepsilon a_0^\dagger$, which gives to leading order as $\varepsilon \to 0$,

$$\frac{\partial n_0^\dagger}{\partial t} + \frac{\partial (v n_0^\dagger)}{\partial z} = \phi\alpha a_0^\dagger - \beta n_0^\dagger, \tag{64}$$

$$\frac{\partial^2 a_0^\dagger}{\partial z^2} = -\phi - n_0^\dagger + (\mu\phi + \lambda) a_0^\dagger, \tag{65}$$

where $n_0^\dagger = p_0^\dagger + q_0^\dagger$, subject to $n_0^\dagger(z,0) = 0$ and $\frac{\partial a_0^\dagger}{\partial z} = 0$ on $z = 0$ and $z = H(t)$. Direct calculation of $n_0^\dagger$ and $a_0^\dagger$ is made awkward by the form of v, leading to a non-uniform distribution of $n_0^\dagger$ due to additional down-regulated cells being introduced through cell birth (since $\gamma = 1$). However, progress can be made by seeking the average density of up-regulated cells, $N_0^\dagger(t)/H(t)$, where

$$N_0^\dagger(t) = \int_0^{H(t)} n(z,t)\, dz,$$

which, from (64), (65) and the boundary conditions, is given by

$$\frac{dN_0^\dagger}{dt} - \Theta_b N_0^\dagger = \phi(\Theta_b + \beta) H, \tag{66}$$

where

$$\Theta_b = \frac{\phi\,\alpha}{\mu\phi + \lambda} - \beta. \tag{67}$$

Direct integration of (66) does not seem to be achievable, but we can deduce from (61) that $\frac{1}{\sqrt{\phi\rho}} \tanh(\sqrt{\phi\rho})\, t \le H(t) \le \frac{1}{\sqrt{\phi\rho}}\, t$, which yields the bound on $N_0^\dagger$,

$$\frac{\tanh(\sqrt{\rho\phi})(\Theta_b + \beta)}{\Theta_b\sqrt{\phi\rho}}(e^{\Theta_b t} - 1 - \Theta_b t) = \underline{N_0^\dagger} \le N_0^\dagger \le \overline{N_0^\dagger} = \frac{(\Theta_b + \beta)}{\Theta_b\sqrt{\phi\rho}}(e^{\Theta_b t} - 1 - \Theta_b t), \tag{68}$$

and $N_0^\dagger \to \overline{N_0^\dagger}$ as $t \to \infty$, since $H \to \frac{1}{\sqrt{\phi\rho}}\, t$ in this limit. The above expansion will breakdown when $n_0^\dagger = O(\varepsilon^{-1})$, implying an $O(1)$ fraction of up-regulated cells being present; a sufficient condition for this is the average $N_0^\dagger/H = O(\varepsilon^{-1})$. The following can be deduced

$\Theta_b > 0$: Significant up-regulation will occur, and the average up-regulated cell fraction $N_0^\dagger/H = O(\varepsilon^{-1})$ on a timescale of $t \sim \frac{1}{\Theta_b}(\ln(1/\varepsilon) + \ln(\ln(1/\varepsilon)))$ as $\varepsilon \to 0$. The low AHL production rate of AHLs by down-regulated cells leads to a delay in noticeable QS activity within the biofilm; however the exponential increase in up-regulated cell density, being faster than the linear biofilm growth, leads to the apparent rapid jump in fraction as depicted in Figure 12 (right).

$\Theta_b < 0$: In large time $N_0^\dagger/H \to$ constant, so the average up-regulated cell density will remain $O(\varepsilon)$ for all time. A more sophisticated analysis is needed to show that $p + q = O(\varepsilon)$, everywhere, but numerics support this notion (not shown).

AHL escape to the surroundings $Q > 0$ is expected to have the effect of increasing the timescale for up-regulation, but the sufficient condition $\Theta_b > 0$ is likely to be relevant.

5.4 Discussion

Presented in this section is a simple model for biofilm growth, quorum sensing and planktonic cell escape. The results show that the largest AHL build up is near the base and in such a way that there is a very rapid jump from a population consisting of near entirely down-regulated cells to one of up-regulated cells and that nutrients can indeed act as a secondary signalling mechanism for changing to the planktonic form. Furthermore, whether or not substantial up-regulation can occur is governed by the parameter Θ_b, which represents a balance between positive QS mechanisms (i.e. up-regulation reaction rate α) and negative mechanisms (such as down-regulation rate β, AHL decay λ and AHL loss by complex formation μ (in dimensionless terms); we note that these parameters are estimatable from routine batch culture type experiments [25] (although how these relate to the biofilm situation is unclear).

However, the existing model does not predict robustly the eventual limiting of biofilm depth; the eventual outcomes could be linear growth (cell birth rate exceeds planktonic escape rate) or finite-time extinction (planktonic escape rate exceeds that of birth). Although simulations involving a slowly growing biofilm reproduce observations reasonably well, the results are very sensitive to the planktonic escape rate constant σ. The model suggests that surface escape of planktonic cells alone cannot lead to the observed depth limitations, and other processes, such as sloughing due to shear forces from the flowing media and/or sporadic degradation and break-up of EPS structure, may play a part. The model presented here is simplistic and can be extended to consider explicitly the water phase, shear forces etc. to model biofilms more realistically; these and other mechanisms will be considered in future studies.

6 Conclusions

In this report several mathematical approaches have been applied to investigate a number of aspects of biofilm growth and development. The models described in Sections 3 and 4 are relevant to general bacterial biofilms, whilst 2 and 5 focussed on aspects more pertinent to *Rhodobacter sphaeroides*. The problems can be summarised as follows

Chain formation: The effects of cell division (whether all cells or just the end cells divide) and chain cleavage (whether cleavage is independent of or increases with chain length) on the steady-state distribution of chain lengths was studied on a Becker-Doring-Smouchowski system. Depending on the combination of the mechanisms a range of qualitatively different distributions result. The mechanisms involved, both biological or physical, are not as yet known; however, comparing chain length distribution data and the size of fragments shed from chains with results from the model could yield information on the mechanical properties of the chain and on the number of bacteria in the chains which are undergoing replication.

Pillar formation: Nutrient-driven instabilities is a well known phenomenon in pillar (usually referred to as finger) formation and the analysis in Section 3 suggests that such instabilities are inevitable in biofilms. In this respect, the elaborate "mushroom-like" structures that form are to be expected and may occur as a consequence of nutrient diffusion limitations alone; although other processes are likely to be significant, such as the flow conditions and EPS production. Furthermore, it is well-known that shear

forces from the fluid media flow effect the morphological development of the biofilm, however, as demonstrated in Section 4, the nutrient distribution resulting from different flow regimes can also have a significant impact on development.

Planktonic cell dispersal and quorum sensing: The modelling demonstrated, as is observed in experiments, that quorum sensing activity is predominant in the substratum regions (due to greater AHL accumulation there) and a sufficient condition for substantial QS activity was established (namely $\Theta_b > 0$). For limiting growth, however, planktonic cell dispersal alone seems to fail as being the dominant mechanism and other volume loss mechanisms are likely to be involved. An interesting experiment would be to investigate whether biofilms of quorum sensing-negative mutants have similar growth limiting properties to the wild-type strains.

Clearly, there is considerably more work that can be done on these and other aspects of biofilm development, but it is hoped that the mathematical modelling presented in this report is instructive and will form the basis of collaborative research in the future.

Acknowledgements

We would like to thank, in alphabetical order, Chris Breward (Oxford), Linda Cummings (Nottingham), John King (Nottingham), Ben MacArthur (Southampton), Philip Maini (Oxford), Eleanor Norris (Loughborough), Simone Severini (York) and anybody else who contributed in the "biofilm suite" or in the bar afterwards.

References

[1] M. Abramowitz & I.A. Stegun. Handbook of Mathematical Functions. Dover, New York, (1972).

[2] D.G. Allison, B. Ruiz, C. SanJose, A. Jaspe & P. Gilbert. Extracellular products as mediators of the formation and detachment of *Pseudomonas fluorescens* biofilms. *FEMS Microbiol. Let.*, **167**, 179-184 (1998).

[3] J.M. Ball & J. Carr. The discrete coagulation-fragmentation equations: existence, uniqueness and density conservation. *J Stat Phys*, **61**, 203–234, (1990).

[4] G.S. Beavers & D.D. Joseph. Boundary conditions at a naturally permeable wall, *J. Fluid Mech.* **30**, 197–207 (1967).

[5] R. Becker & W. Döring. Kinetische behandlung der keimbildung in übersättigten dämpfen. *Ann Phys*, **24**, 719–752, (1935).

[6] N.V. Brilliantov & P.L. Krapivsky. Non-scaling and source-induced scaling behaviour in aggregation models of movable monomers and immovable clusters. *J Phys A; Math Gen*, **24**, 4787–4803, (1991).

[7] J.W. Costerton, Z. Lewandowski, D. DeBeer, D. Caldwell, D. Korber & G. James. Biofilms, the customized microniche. *J. Bact.*, **176**, 2137-2142 (1994).

[8] J.W. Costerton & Z. Lewandowski. Microbial Biofilms. *Ann. Rev. Microbiol.*, **49**, 711-745 (1995).

[9] H. Dang & C.R. Lovell. Bacterial primary colonization and early succession on surfaces in marine waters as determined by amplified rRNA gene restriction analysis and sequence analysis of 16S rRNA genes. *Appl. Environ. Microbiol.*, **66**, 467-75. (2000).

[10] M.E. Davey & G.A. O'Toole. Microbial biofilms: from ecology to molecular genetics. *Microbiol. Mol. Biol. Rev.*, **64**, 847-867 (2000).

[11] J. Dockery & I. Klapper. Finger formation in biofilm layers, *SIAM J. Appl. Math.* **62**, 853–869 (2002).

[12] C. Fuqua, S.C Winans & E.P. Greenberg. Census and consensus in bacterial ecosystems: the luxR-luxI family of quorum-sensing transcriptional regulators. *Ann. Rev. Microbiol.* **50**, 727-751 (1996).

[13] C. Fuqua & E.P. Greenberg. Self perception in bacteria - quorum sensing with acylated homoserine lactones.. *Opin. Microbiol.*, **1**, 183-189 (1998).

[14] J.R. King & J.A.D. Wattis. Asymptotic solutions of the Becker-Döring equations with size-dependent rate constants. *J Phys A; Math Gen*, **35**, 1357–1380, (2002).

[15] J.R. Lawrence, D.R. Korber, B.D. Hoyle, J.W. Costerton & D.E. Caldwell. Optical sectioning of microbial biofilms. *J. Bact.*, **173**, 6558-6567 (1991).

[16] R.J.C. McLean, M. Whiteley, B.C. Hoskins, P.D. Majors & M.M. Sharma. Laboratory techniques for studying biofilm growth, physiology, and gene expression in flowing systems and porous media. *Meth. Enzymol.*, **310**, 248-264 (1999).

[17] M. Mimura, H. Sakaguchi, & M. Matsushita. Reaction-diffusion modelling of bacterial colony patterns. *Phys. A*, **282**, 283-303 (2000).

[18] H.L. Packer & J.P. Armitage. Behavioral responses of *Rhodobacter sphaeroides* to linear gradients of the nutrients succinate and acetate. *Appl. Environ. Microbiol.*, **66** , 5186-5191. (2000).

[19] J.R. Palmer & D.C. White. Developmental biology of biofilms: implications for treatment and control. *Trends microbiol.*, **5**, 435-440 (1997).

[20] C. Picioreanu, M.C. M. van Loosdrecht & J. J. Heijnen. A theoretical study on the effect of surface roughness on mass transport and transformation in biofilms, *Biotech. Bioeng.* **68**, 355-369 (2000).

[21] A. Puskas, E.P. Greenburg, S. Kaplan & A.L. Schaffer. A quorum-sensing system in the free-living photosynthetic bacterium *Rhodobacter sphaeroides*, *J. Bact.* **179**, 7530-7537 (1997).

[22] C. Reimmann, M. Beyeler, A. Latifi, H. Winteler, M. Foglino, A. Lazdunski & D. Haas. The global activator GacA of *Pseudomonas aeruginosa* PAO positively controls the production of the autoinducer N-butyryl-homoserine lactone and the formation of the virulence factors pyocyanin, cyanide, and lipase. *Mol. Microbiol.*, **24**, 309-319 (1997).

[23] M. von Smoluchowski. Drei vorträge über diffusion, brownsche molekular bewegung und koagulation von kolloidteichen. *Physik Z*, **17**, 557, (1916).

[24] G.H. Wadhams, A.C. Martin, A.V. Warren & J.P. Armitage. Requirements for chemotaxis protein localization in *Rhodobacter sphaeroides*. *Mol. Microbiol.*, **58**, 895-902 (2005).

[25] J.P. Ward, J.R. King, A.J. Koerber, P. Williams, J.M. Croft & R.E. Sockett. Mathematical modelling of quorum sensing in bacteria, *IMA J. Math. Appl. Med. Biol.* **18**, 263-292 (2001).

[26] P. Watnick & R. Kolter. Biofilm, City of Microbes. *J. Bact.*, **182**, 2675-2679 (2000).

[27] J.A.D. Wattis & P.V. Coveney. The origin of the RNA world: a kinetic model. *J Phys Chem*, **103**, 4231-4250, (1999).

[28] J.A.D. Wattis & J.R. King. Asymptotic solutions of the Becker-Döring equations. *J Phys A; Math Gen*, **31**, 7169-7189, (1998).

[29] J.W.T. Wimpenny & R. Colasanti. A unifying hypothesis for the structure of microbial biofilms based on cellular automaton models. *FEMS Microbiol. Ecol.*, **22**, 1-16 (1997).